CHARACTERIZATION OF INTERFACIAL BOND STRENGTH IN FIBER REINFORCED CEMENTITIOUS COMPOSITES BY A MODIFIED PULLOUT METHOD

A Thesis
Submitted to the Graduate Faculty
of the
North Dakota State University
of Agriculture and Applied Science

By

Rajender Reddy Chada

In Partial Fulfillment of the Requirements
for the Degree of
MASTER OF SCIENCE

Major Department:
Construction Management and Engineering

November 2017

Fargo, North Dakota

North Dakota State University

Graduate School

Title

CHARACTERIZATION OF INTERFACIAL BOND STRENGTH IN FIBER REINFORCED CEMENTITIOUS COMPOSITES BY A MODIFIED PULLOUT METHOD

By

Rajender Reddy Chada

The Supervisory Committee certifies that this ***disquisition*** complies with North Dakota State University's regulations and meets the accepted standards for the degree of

MASTER OF SCIENCE

SUPERVISORY COMMITTEE:

Dr. Todd Sirotiak

Chair

Dr. Ravi Kiran Yellavajjala

Dr. Matthew Stone

Approved:

11/15/2017	Dr. Jerry Gao
Date	Department Chair

ABSTRACT

This document entails the research work carried out to propose a new method for quantifying the interfacial bond strength in fiber reinforced cementitious composites. A modified pullout test has been designed to determine the interfacial bond parameters for natural fibers with cementitious system, and were repeated for artificial fibers for comparison studies. Steel, polypropylene, and wheat straw fibers were tested with the modified pullout method. Surface roughness studies were conducted on the same fibers to establish a relationship between the roughness index of fibers and corresponding bond strengths evaluated from the new method. Also, standard single fiber pullout tests were conducted for steel and polypropylene fibers. The pulled-out fibers were further analyzed using scanning electron microscopy and energy dispersive spectroscopy in conjunction. Peel test, an experimental study was also discussed in this research.

ACKNOWLEDGMENTS

I would like to acknowledge everyone who has been a part of my graduate life for the past two years to have made this possible. Firstly, I'd like to thank my graduate committee members, Dr. Todd Sirotiak, Dr. Ravi Kiran Yellavajjala, and Dr. Matthew Stone for immense support and unconditional guidance throughout my research work. I'd also like to thank DTI group graduate students for helping me out with my research study. A special thanks to NDSU Research Park facility lab technicians Fred Haring and Greg Strommen for having the time and patience to train me on the research equipment. I would also like to extend my gratitude towards Jayma Moore and Scott Payne from NDSU electron microscopy center, for assistance with SEM and EDS analysis. Finally, I wish to acknowledge Dr. Dayakar Naik Lavadiya, for being an integral part of my research work and thesis writing.

DEDICATION

I would like to dedicate this thesis to my mom, dad, and my brother who've stood by me through thick and thin of my life.

TABLE OF CONTENTS

LIST OF TABLES

LIST OF FIGURES

LIST OF APPENDIX TABLES

INTRODUCTION AND BACKGROUND

Fiber reinforced composites are widely used in current construction scenario for various purposes. The idea of using fibers as a blend to make a composite building material dates back to ages. Straw fibers were mixed with bricks for reinforcement before sun-baking them, in Baghdad about 3500 years ago (Swamy, 1980) and asbestos fibers were similarly used in early 1900's as a reinforcing component for building materials (ACI commitee, 2005). Although there was a glimpse of research in earlier centuries into the use of fibers in building and construction materials, it was not until the 1960's that fiber reinforcement for concrete had started to gain popularity (Nepal, 2015). Fiber reinforced cementitious systems are currently used in the construction industry for such purposes as airport and high way overlays, pavements, corrugated sheets, pile caps, and light weight wall panels (ACI commitee, 2005) (Bentur & Mindess, 2006). Such fiber reinforced systems have a refined structural integrity, with improved tensile and flexural strengths, higher impact energy absorption, wear durability, and toughness. The primary objective of blending fibers in cementitious composites was to investigate their ability to enhance a cementitious system's mechanical properties. In previous research studies the primary concern found in cement and concrete composites was their weakness in resistance to cracking under load. The brittle nature of cement has consistently provided a scope for perpetual research toward solutions to modify and improve the material's ductility and tensile strength (Onuaguluchi & Banthia, 2016) (Bentur & Mindess, 2006) (Nepal, 2015). This is where fibers have been introduced as a reinforcement, showing a promising future in the construction industry and evolving over the years to an importance place in the field today.

Fiber reinforced cementitious composites are a well-blended system of discrete and discontinuous fibers in Portland cementitious systems (paste, mortar, or concrete). The

cementitious system which acts as a medium for the fibers is often termed a matrix. Various fibers were used in cement composites which can be put into natural or artificial fibers on a broad classification basis. Cementitious systems reinforced with artificial fibers have exhibited greater improvements in tensile strength and cracking control when compared to those reinforced with natural fibers (Onuaguluchi & Banthia, 2016). Fibers have known to impart high mechanical strength in the cement composites as an effect of their physical and chemical characterization. Resistance against cracking, improvements in tensile strength, and increased toughness are attributes of a fiber's chemical and mechanical bonding behavior with a cementitious composite i.e., enhancement in mechanical strength of the fiber reinforced cement composites is a behavioral trait of bonding between the fiber and matrix (Wei, Mandel, & Said, 1986). The interface in a composite is a region that acts as a transition phase between the fiber and matrix and determines the bond strength in the composite. Fiber-matrix studies in the past have shown a need for microstructural investigation of the fiber-matrix interface in a composite system to understand the bond behavior and thereby evaluate the interfacial bond parameters associated for the composite (Bentur & Mindess, 2006) (ACI commitee, 2005) (Wei, Mandel, & Said, 1986). Fracture mechanics in the fiber cementitious systems were studied to learn about the interfacial bond properties in the composite and their impact on the mechanical properties of the composite. Micromechanical studies along fracture planes in fiber cementitious systems have shown that crack resistance is offered by the bridging behavior of the fibers. Better tensile strength results for fiber cementitious composites were also due to the bridging capability of fibers across microcracks (Chamis, 1972).

The principle theory behind the improvement of the composite mechanical performance with added fibers lies in the exploration of the micromechanical study at the fiber/matrix interface.

Although load transfer in a fiber reinforced composite is different in pre-cracking and post-cracking stages, the principle mechanism is energy absorption transfer from matrix to fiber when strained. Since the fiber and matrix have different elastic moduli, there is an uneven strain energy absorption in the composite system's components when stressed (Wang, Li, & Backer, Modeling of fiber pull-out from cement matrix, 1988) (Bentur & Mindess, 2006). Typically, in the post-cracking stage fiber-matrix composites have showed a crack propagation at the interface when load was acted upon them. As a microcrack appears at the point of loading in a cementitious system, the fracture spreads until a fiber surfaces across the fracture plane and acts as a medium for energy absorption by transferring it from the composite. The ability of the interface to propagate the crack from the matrix to the fiber along the surface of the interface depends upon the interfacial bond strength. In simpler words, the load transfer capability at the interface from matrix to fiber strengthens the composite in resisting the crack (Chamis, 1972). There is an energy consumption involved with this process that is also a controlling parameter of the composite's toughness deciding the interfacial bond characterization.

Interfacial bond strength of the fiber reinforced composites is due to the adhesive bond characterized by the chemical bonding between fiber and matrix, and the frictional bonding that comes with mechanical interaction of the fiber with matrix at the interface (Naaman & Shah, 1976). The latter is dependent upon the mechanical interlocking of the fiber and hence depends upon the physical characteristics of the fiber and matrix (Marshall & Cox, The mechanics of matrix cracking in brittle-matrix fiber composites, 1985). Existing methods of interfacial bond strength measurement works on the basic mechanism of relative displacement of the fiber with matrix at the interface, and therefore measuring the force needed to debond the fiber from the matrix gives the value for interfacial bond strength. Even though there has been a significant development in

methods for measuring the interfacial bond strength of a fiber/matrix in thermoplastics, single fiber pullout tests were the only possible method for evaluating interfacial bond strength in fiber reinforced cementitious composites. Determination of bond strength was more complex than it seemed from the initial pullout methods developed, due to the different assumptions made in them which indicated an inefficient way of corresponding fiber contribution in the composite (Naaman & Shah, 1976). The standard pullout test evolved over the years works on the basic principle of pulling a specific length of fiber out of matrix to record the load required and thereby making an analysis for the shearing of fiber against matrix. Test specimens prepared typically for a pullout test have fiber partly embedded in the matrix for some length which is termed as embedment length. The matrix is held steady in its place during the pullout of the fiber from the test specimen. The embedded end of the fiber is displaced relative to the original position that was considered as fiber slippage in the test. The test curves plotted for the recorded loads against the fiber slip produce the pullout curves from which the interfacial bond parameters can be evaluated.

Current pullout analysis for the curves was developed from the traditional models analyzed in early pullout research studies. Semi-synthetic and synthetic fibers have been analyzed differently for their pullouts in previous research works owing to the different bond-slip mechanisms they exhibit. Initial studies for pullout were performed for matrix surfaces with more than single fiber to study the practicality of load transfer at the fracture surface in a fiber reinforced composite, before the direct pullout models were proposed (Wang, Li, & Backer, Modeling of fiber pull-out from cement matrix, 1988) (Wang, Li, & Backer, Analysis of synthetic fiber pull-out from cement matrix, 1987) (Naaman & Shah, 1976). Pullout models developed in literature have been analyzed either on their strength control or fracture control mechanism. The generalized modeling of fiber pullout was done neglecting Poisson's effect (i.e., radial contraction of the fiber

during pullout) (Wang, Li, & Backer, Analysis of synthetic fiber pull-out from cement matrix, 1987). The fracture control mechanism used for pullout problem solving analyzes the load transfer from matrix to fiber in the composite, where the interfacial parameters evaluated were the peak load that can be withstood by the fiber during pullout, and the energy absorption involved in the process of the pullout (Chamis, 1972) (Leung & Li, 1990). The pullout process is depicted typically by plotting curves for the pullout load recorded vs slip in the embedded end of the fiber.

The interfacial bond between fiber and matrix is typically a mixture of adhesive/ elastic bonding due to chemical interaction, and frictional bonding due to mechanical interaction between the fiber and matrix (Bentur & Mindess, 2006) (Chamis, 1972) (Wei, Mandel, & Said, 1986). When the fiber is undergoing pullout test from the matrix, it debonds elastically before the pullout of the fiber starts. Early studies have assumed an elastic nature for a fiber-matrix interface which yielded to a uniform elastic and frictional bond through the pullout process, which was later corrected for the brittle nature of cementitious matrix. The frictional pullout process was remodeled with consideration for the variable frictional stress post elastic debonding phase (Wang, Li, & Backer, Modeling of fiber pull-out from cement matrix, 1988). The pullout energy associated with the pullout process is a vital component that characterizes the composite's toughness in post-cracking stage (Alwan, Naaman, & Hansen, 1991). Energies associated with elastic debonding and frictional pullout were calculated by evaluating the area under the pullout test curves and pullout energy in a composite is dependent on various factors such as fiber embedment length, fiber aspect ratio, initial frictional bond shear stress, bond modulus, and the damage coefficient (Alwan, Naaman, & Hansen, 1991). The peak pullout load transfer at the fiber-matrix interface in a cementitious composite determines the limit of the composite to undergo tension in post-cracking stage. Hence, it is essential to design composites with high values of peak pullout load and pullout

energy to obtain required crack resistance and toughness (Wei, Mandel, & Said, 1986). The pullout studies conducted account for variables such as the angle of inclination of the fiber pullout, the volume content of fibers, and the water cement ratio in the composite, all of them important factors for the pullout resistance (Naaman & Shah, 1976) (Wei, Mandel, & Said, 1986) (Abu-Lebdeh, Hamoush, Heard, & Zornig, 2011). Pullout modeling studies later identified further factors such as typical geometry and aspect ratio of the fibers, mechanical deformations in the fibers in the composite during manufacturing, surface treatment on the fibers, and the rate of crosshead applied for the pullout testing to be influential in the analysis (Li, Wang, & Backer, 1990) (Abu-Lebdeh, Hamoush, Heard, & Zornig, 2011) (Abbas & Khan, 2016) (Babafemi & Boshoff, 2017) (Banthia & Trottier, 1994) (Gokoz & Naaman, 1981) (Zile & Zile, 2013) (Choi & Lee, 2015) (Pacios, Ouyang, & Shah, 1995) (Fantilli & Paolo, 2007). Studies conducted recently for fiber pullouts from high and ultra-high performance cementitious systems have reported significant difference from ordinary cementitious system pullout (Abu-Lebdeh, Hamoush, Heard, & Zornig, 2011) (Jewell, Mahboub, Robl, & Bathke, 2015) (Naaman & Willie, 2012), which indicates that the particle packing density in the matrix has an effect on the pullout resistance.

Pullout studies on steel and synthetic fibers have demonstrated necessity for increasing bond properties to increase the fiber reinforced cementitious composite's mechanical performance. Steel pullout tests were extensively analyzed from the 1960s to the 1990s until synthetic fibers have started to gain interest. Being hydrophilic, steel fibers have a peculiar transitional phase formed with cementitious systems when mixed. The interface was observed to have the water content from a cementitious system percolated around the large hydration products of fresh cement paste that makes it easier for steel fiber to be pulled out (Katz, Bentur, Alexander, & Arliguie, 1998). A lower water cement ratio during the mix has shown a higher value for the steel fiber

cement composite's tensile strength improvements (Wei, Mandel, & Said, 1986). Steel fiber pullout analysis has shown that with increase in the embedment length of the fiber and fiber volume fraction in the composite, the peak pullout loads, and the pullout energies increased (Shannag, Brincker, & Hansen, 1997). Naaman et al. have also investigated the pullout work as a function of debonding work in the pullout phase, and concluded that the major mechanism contributing to total energy absorption in the pullout test was frictional pullout. It was observed that the steel fibers' microhardness was higher compared to the cementitious matrix, due to which the steel fiber pullout exhibits a decreasing frictional stress with increasing fiber slippage as the debris of ruptured matrix material decreases the bond surface area at the interface (Alwan, Naaman, & Hansen, 1991) (Li, Wang, & Backer, 1990) (Shannag, Brincker, & Hansen, 1997). This phenomenon is also called the slip softening effect and is commonly seen for steel fiber pullout test curves (Li, Wang, & Backer, 1991). Improvements in mechanical performance for steel-cement composites were also related to particle dispersion in the cementitious system (i.e., a high strength or a densely packed cement system has shown high pullout loads and energies associated with the pullout test) (Abu-Lebdeh, Hamoush, Heard, & Zornig, 2011) (Naaman & Willie, 2012). Another investigation into currently available deformed fibers puts forward evidence for an additional mechanical anchorage provided at the interface by design engineering of the manufacturing process, which in turn depends upon fiber geometry and yield stress (Abbas & Khan, 2016) (Zile & Zile, 2013) (Banthia & Trottier, 1994).

Synthetic fibers have shown that frictional stress during the pullout phase increases because of softer surface characteristics. The microhardness of synthetic fibers being lower than that of cementitious matrix, they are abraded by the cement matrix leading to an increase in the surface area of the fiber to bond in the pullout phase, which explains the increasing frictional shear stress

with respect to increasing fiber slippage in the pullout test (Katz, Bentur, Alexander, & Arliguie, 1998). This effect is commonly termed as slip hardening and is typically seen in synthetic fiber pullout test curves (Kanda & Li, 1998) (Babafemi & Boshoff, 2017) (Singh, Shukla, & Brown, 2004) (Wang, Li, & Backer, Modeling of fiber pull-out from cement matrix, 1988). Surface abrasion of fibers has resulted in higher pullout loads and pullout energies (Wang, Li, & Backer, Analysis of synthetic fiber pull-out from cement matrix, 1987). Wang et al. have provided a theoretical model for the analysis of synthetic fiber pullout from cement matrix considering a non-uniform bond strength along the slip of the fiber. Synthetic fibers have displayed an unconventional characteristic of a probable increase in resistance towards cracking with an increase in the inclination angle of fibers with the matrix, but limited (Li, Wang, & Backer, 1990). It was seen that the bundling effect of fibers correlates with a decrease in the effectiveness of a synthetic fiber's reinforcement. (Wang, Backer, & Li, An experimental study of synthetic fiber reinforced cementitous composites, 1987). A research study on polyvinyl fiber pullout tests has indicated high chemical bond strength values in comparison to frictional bond strength (Kanda & Li, 1998). Synthetic fibers show an increase in their pullout loads and pullout energies with an increase in their embedment length and with modifications in their surface characteristics. It was found in a study, that the microstructure of the cement matrix plays a significant role in determining the interfacial bond parameters in pullout tests (Babafemi & Boshoff, 2017) (Singh, Shukla, & Brown, 2004). Pullout tests studied also indicated that synthetic fibers are efficient in the pullout method for an analysis during early stages of curing of cementitious matrix (Jewell, Mahboub, Robl, & Bathke, 2015). Variables influencing bond behavior need to be minimized when research involves different classes of fibers.

RESEARCH SIGNIFICANCE

Synthetic fibers have generally higher peak tensile strength and elastic modulus values than natural fibers and, hence higher enhancement of mechanical properties in cement composites. Synthetic fibers are typically hydrophobic in nature, which makes their mechanical properties resistant to degradation over time unlike those of natural fibers (ACI commitee, 2005). However, these materials require longer degradation time periods compared to natural fiber reinforced cement composites. Natural fibers are larger that synthetic fibers in their diameters and aspect ratio. A fiber's aspect ratio has proved to be the determining factor in deciding the fresh paste properties of fiber reinforced cement composite such as, workability and air content (Bentur & Mindess, 2006). Fiber's microstructure plays a key role in mechanical bonding with the cementitious system thereby controlling the cracking resistance of the composite. The use of plant and agricultural fibers has gradually increased over the past few decades (Onuaguluchi & Banthia, 2016) (Nepal, 2015). The challenges that arise with use of natural fibers in cement composites were considered and consequently, many studies have shown that with surface treatments, shape and size modifications, natural fibers could be an adequately reinforcing material for lighter construction purposes. Natural fibers have recently been replacing synthetic fibers in applications that need moderate mechanical strength, due to their low cost, renewability, decent tensile and flexural strength, and biodegradability (Onuaguluchi & Banthia, 2016). These fibers primarily contain, cellulose, hemicellulose, lignin, and other organic waxes. One of these of these organic compounds or a combination of them in natural fibers cause the presence of waxy layers on their surfaces tending them hydrophobic (Nepal, 2015). Natural fibers exhibit a roughened physical surface underneath their waxy layers which hinders the adhesive capability of the fiber with the matrix. Surface treatments for natural fibers have improved their surface characteristics leading to

a stronger bridging behavior of fiber with matrix (Bentur & Mindess, 2006). Surface treatments for natural fibers included acetalization, alkalization, and treatment with silane coupling agents, removing waxy layers formed by cellulose hexagon chains and then treatment with an agent to makes the outer surface hydrophilic. However, treated natural fibers exhibit a change in their chemical composition that renders the mechanical strength values examined inaccurate. A suitable treatment for natural fibers is essential, in order to cause a significant change in the physical nature of the fibers without disturbing their chemical composition. Most treated natural fibers studied in the past such as sisal, kenaf, pineapple, wheat and rice straw, and coconut have exhibited coarse profiles and have shown greater improvements in composite mechanical strength when compared to untreated fibers (Onuaguluchi & Banthia, 2016). Though single fiber pullout tests were widely performed to evaluate interfacial bond behavior in fiber reinforced cementitious composites, such tests were never performed for natural fibers due to their low tensile strength. A fiber rupture is highly probable before the fiber is pulled out, owing to the low peak tensile strength of the natural fibers. In this research study, there was a new method developed to evaluate the mechanical bond strength of natural fibers with a fresh cementitious system and mechanical bond strength of natural fibers was studied as a characteristic of surface roughness. Hence, a comprehensive study of modified pullout method was done in this study along with its validation.

MATERIALS AND TESTING METHODS

Modified Pullout Method

Three different sets of fibers were tested with the new methodology for evaluating their interfacial bond strengths with cementitious matrices. Steel and polypropylene fibers used in this research work were obtained from different manufacturers. The natural fiber tested for the new method was wheat straw fiber that were procured from a local agriculture field on campus at North Dakota State University. Figures 1, 2, and 3 show pictures of steel, polypropylene and wheat straw fibers, respectively used for the experimental purposes. A table itemizing their physical and chemical properties was also provided, refer to table 1. Tests for evaluating the fiber mechanical properties were later discussed in detail. Steel and polypropylene fiber cross-sections were observed to be rectangular. To make a generalized evaluation as per literature for bond parameters in the results section, the rectangular cross-sections were replaced by circular cross-sections of the same area. This was done only to make quantitative evaluations for bond parameters.

Figure 1. Steel fibers

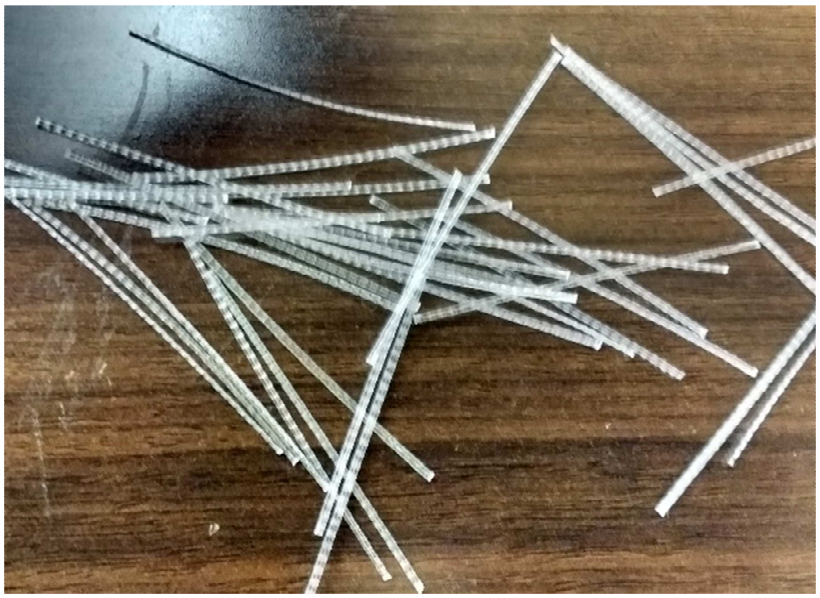

Figure 2. Polypropylene fibers

Figure 3. Wheat straw

Table 1

Properties of experimented fibers

Properties	Stainless Steel	Polypropylene	Wheat Straw
Length	25mm	54mm	Chopped to 50mm
Typical Aspect Ratio	50	70	27
Equivalent diameter	0.5mm	0.77mm	1.897mm
Quantity per Kg	24,000	43,700	-
Specific Gravity	7.87	0.91	-
Tensile Strength	524MPa	585MPa	47.06MPa
Corrosion Resistance	Good	Excellent	-
Melting Point	1450^0C	160^0C	-
Elastic Modulus	33,695MPa	14,200MPa	3,886MPa

As for the modified pullout method matrix, a cement clay mixture was prepared for pullout experimentation. For this mixture Portland Type 1 cement, Ceramic Clay Flour, and water were mixed in a Flacktek Speed mixer in 1:1:1 ratio by volume. Trial mixes were made with many other ratios, but no information in the literature conformed the mix design to a specific code. The best mix design was attained by checking for cement clay paste consistency over some time, post mixing. Portland Type 1 cement used for the new method was obtained from the concrete laboratory at NDSU. A natural gray ceramic clay flour was purchased from AMACO (American Art and Clay Company) in dry powder form which is typically used for hand modeling and household purposes. This dry clay flour serves as an admixture that improves the consistency of the cement paste when mixed with water and maintains a constant value over a period of time (found to be around 30 minutes in trial mixes). The equal volume ratio of water to cement and clay

can be explained by the absorption capacities of both dry powders. Portland cement requires almost 48.5% of water by volume as per ASTM standards, and clay requires around 50-55%, making it a safer estimation to go with a 100% volume of water for the cement clay mixture. A Flacktek speed mixer (as shown in Figures 4 and 5) - is capable of mixing small loads up to 100g and was used for mixing the three components. Equal volume quantities of Portland type 1 cement, clay and water were measured in three identical containers and added into one container, and closed with a lid before mixing, and then placed in the Flacktek mixer calibrated to run at 33rpm for two minutes. After mixing, the lid was opened, and the cement clay paste was checked for homogeneity. This mix was immediately transferred into the pullout specimen mold for further experimentation.

Figure 4. Flacktek mixer

Figure 5. Inside view of mixer

A 3D printed fixture was used as a mold for the cement clay mix prepared in the Flacktek mixer. The geometry of the mold was formulated so as to accommodate the quantity of mix, and the structural stability of the fixture between the grips of the testing machine while operating. The ingredients comprised in the resin used for preparing this 3D mold were methacrylate oligomers, methacrylate monomers, and photo initiators. The mold post 3D printing was cured for one day under ultraviolet light to achieve the desired strength and toughness. The 3D mold was schematically comprising of two sections, the top part a hollow cylinder with the top face open acting as a mold for the mix. The bottom part was a dense cuboid section connecting to the bottom face of the top part that acts as a fixture between the grips for testing equipment. This 3D mold weighed around 225g with a total volume of 28,670mm^3 and surface area of 11840mm^2. The top section of cylindrical vessel was 60mm long with an outer radius of 25mm and an inner radius of 15mm which provides a space of 9200mm^3 approximately. As mentioned earlier, the cement clay mixture is prepared in Flacktek mixer for two minutes followed by the pouring of this mix into the

3D mold. While the medium is being transferred from the speed mixer container to the mold, precautions were taken in order to avoid air voids in the specimen by tamping the paste poured in the mold in two intervals. Additionally, the surface area inside the cylindrical portion was made completely dry to validate the water-cement clay paste ratio remaining constant for all specimens prepared. Finally, after the test specimen was prepared, fiber was introduced into the medium at right angles to the cross-sectional plane of the matrix and was embedded into it for a certain length. The specimen preparation took about an average 10 minutes of time after the mixing was done. This specimen was then tested for pullout of the fiber in the Instron tensile testing machine with a maximum load capacity of 500N, under a load cell of 100N at a displacement rate of 1.00 mm/min. The instrument was calibrated for the first specimen and then operated at a constant displacement rate for eight specimens each for steel, polypropylene, and wheat straw fibers for two different lengths 10mm, 20mm, that sump up to a total of 48 test specimens.

Figure 6. 3-D printed mold

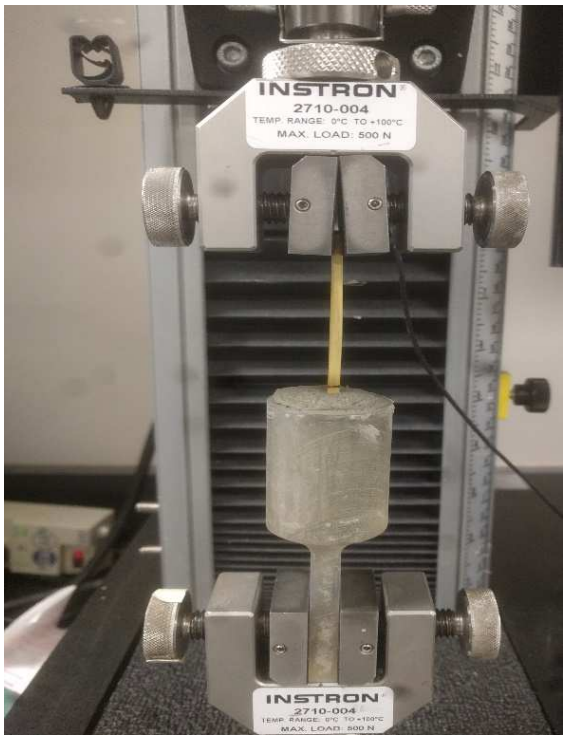

Figure 7. Test setup for modified pullout method

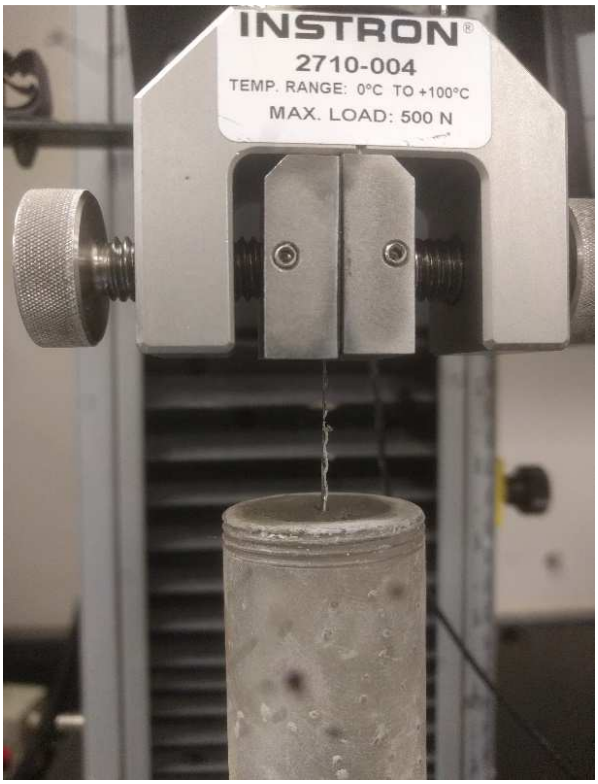

Figure 8. Steel fiber pullout

Figure 9. Steel fiber post pullout

Conventional Single Fiber Pullout Tests

Single Fiber Pullout tests were performed on various fiber reinforced composites in the literature. In this research work, pullout tests for steel and polypropylene fibers from cementitious matrices were conducted in a way similar to that performed in earlier studies. The same fibers used in modified pullout method tests were used for this method. Single fiber pullout tests were performed on a Shimadzu testing machine with a maximum load capacity of 5KN. Test specimens were prepared using Portland type 1 cement, sand, and fibers. Initially, Mortar mixing was done as per ASTM standards with w/c ratio of 0.485. This prepared mortar mix was poured into cube molds of size 50mm by 50mm followed by 10mm embedment of the fiber into the cube at the center of the top face. These specimens were air cured for one day and then placed in a water tank for seven days curing. There were seven cubes each prepared for each fiber type, for a sum of 14 single fiber pullout test specimens. Refer to Figure 11 for a typical pullout specimen prepared with

10mm embedment length. The testing technique of the cured test specimens on the machine requires a fixture that accommodates the pullout specimen and fits into the lower grips of the machine under operation. Since the fixture had to withstand the pullout force on the specimen during the test, Steel was chosen for the material. A hollow rectangular steel tube of 60mm x 50mm cross-section with a thickness of 3mm, and a 5ft L-shaped steel angle of 50mm arm width, thickness of 2mm were bought from a local store. Two minor angles of 50mm length were cut from this L section and welded back to back to form a T shaped section. 50mm length of the tube was cut from the whole section and its bottom surface was welded to the T-shaped angular section prepared earlier as shown in Figure 10. The final structure attained weighs about 600g, and looks like a hollow box. There are two faces open on the sides of this box for mounting the pullout specimen attached to a dense linear section of 6mm thickness beneath the box that fits into the testing machine grips as shown in Figure 12. The steel test fixture was also provided with an open slit on the top face to allow the fiber to pass through and is held by the top grips of the machine.

Figure 10. Steel fixture

Figure 11. Single fiber pullout test specimen

The Pullout tests were performed on a universal testing machine Shimadzu EZ-LX series model with a maximum load capacity of 5KN. The UTS was operated under a load cell of 1KN at a constant displacement rate of 1.00mm/min for all test specimens. After introducing steel fixture into the bottom grips, it is tightened enough to hold it steady and the upper wedge of the machine is lowered such that it lies near the top face of the steel fixture. The top surface of the mortar cube specimen which would be in contact with the steel fixture was smoothened, to maintain a uniform contact throughout the surface area before pullout. The fiber pullout cube specimen was introduced into the steel fixture through the open slit end side, making sure the cube is held tightly with its top face touching the steel fixture surface, followed by screwing the fiber into the top grips tightly. Cautiously, the top grips were made to hold the maximum length of the fiber between their jaws right on top of the slit, almost touching the surface of steel fixture in order to avoid any localized stress formations (as well as Poisson's effect) in the fiber while being pulled out. Since the cubes were 5mm shorter than the steel fixture, they would be hanging inside the cavity with fiber gripped

between the jaws of top grips. The instrument was calibrated for immediately after specimen mounting by correcting the load and extension to zero. The fiber pullout instrumentation was started right after the calibration and was visually recorded with a smartphone camera. The mortar cube drops down onto the bottom surface of the steel cavity while the fiber is held between the grips at the end of the pullout process. After the fiber gets pulled out, the test was saved in the Trapezium X software which provides tester access to exporting the raw data. Pulled out fibers leave a hole in the mortar cubes after testing. The cubes and fibers after pullouts were collected and stored for further analysis. Pulled out fibers were analyzed using SEM and EDS in conjunction.

Figure 12. Steel fixture mounted into Shimadzu

Figure 13. Test setup for standard pullout

Mortar cubes collected after pullout testing were cut with a diamond saw cutter along five planes. There were four planes running perpendicular to the top face and running parallel to the four sides of the cube at 3mm distance from the center of the hole, as well as one cutting plane perpendicular to the depth of the hole that runs parallel to the top face of the cube at 12mm length. This process produced a miniature version of the pullout cubes. Micro CT analysis was done for these miniature cube specimens.

Peel Test

This test was an experimental pilot study to measure the peeling strength of the steel and polypropylene fibers with cement matrix. A common test for adhesives, used to test the bond strength of a material when peeled from the surface of another material was replicated in this work. Peel test specimens were prepared using Portland type 1 cement, sand, water, and fibers. The preparation of peel test specimens was similar to that of single fiber pullout test specimens. Mortar

was prepared by mixing cement, sand, and water as per ASTM code standards followed by pouring the mix into 50mm x 50mm cube molds. After finishing the mortar smoothly, a 1 mm depth fissure was drawn on the top surface for a length of 5mm starting from the midpoint of an edge going inwards to the center of the face. Fiber was carefully placed in the resulting ditch, such that 5mm of the fiber was lying on the top surface of the mortar while the rest of it was hanging free. There were ten cubes casted with five each for steel, and polypropylene fibers. After arranging the fibers in the cubes, they were covered with plastic sheets for 24 hours. The cubes were then demolded and cured in water for seven days. After removing the cubes from the curing tank, they were ready to be tested for peel strength as shown in Figures 14 and 15. The cubes were tested on the same UTS Shimadzu that was used for single fiber pullout tests, with the same steel fixture. But, since the fiber was bonded unsymmetrically to the medium there were some counter weights used below the cube while testing. Test specimens were mounted into the steel fixture system with fiber standing vertical for the jaws to grip them. The test specimens were hand held tightly to avoid any space between the top face of the cube and steel surface while the grips were tightened. Once the fiber was gripped tight, counter weights were placed underneath the cube and hands were taken off the cube for testing, refer Figure 16. These cautions ensured that the test specimen underwent proper peeling throughout the peel length of the fiber. If counterweights weren't provided, the cube would have taken an inclined position with the end to which fiber attached end on top, due to which the fiber tends to shear off from the matrix instead of peeling consistently.

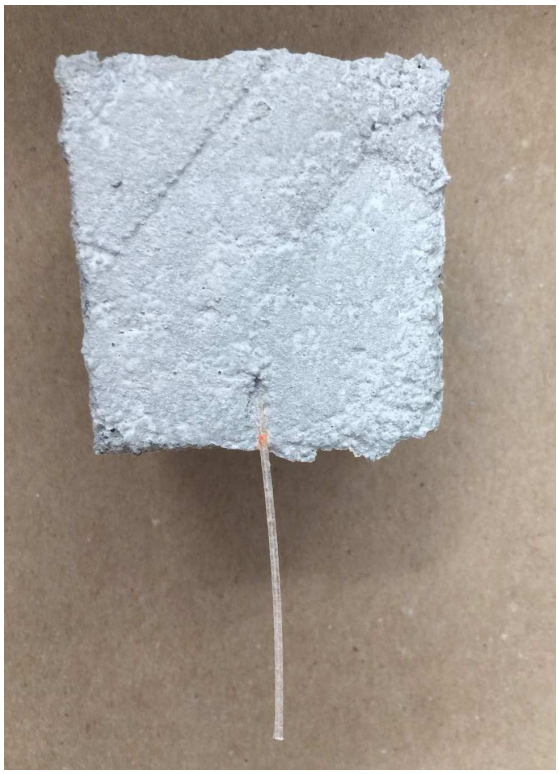

Figure 14. Top view of peel test specimen

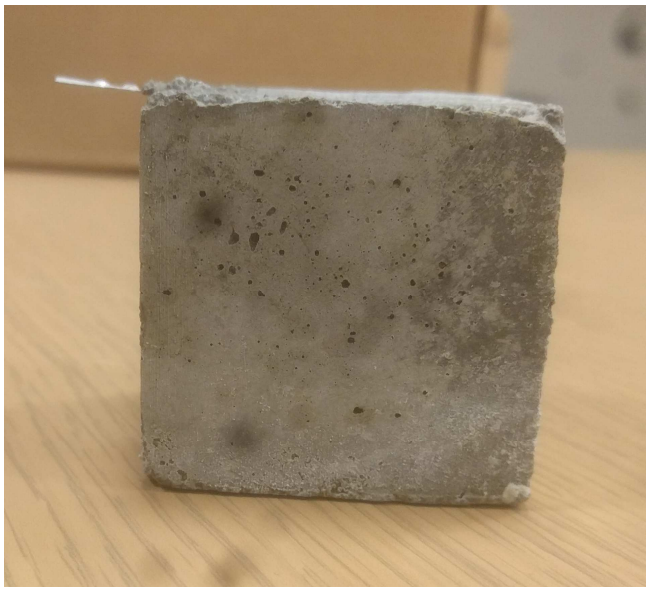

Figure 15. Side view of peel test specimen

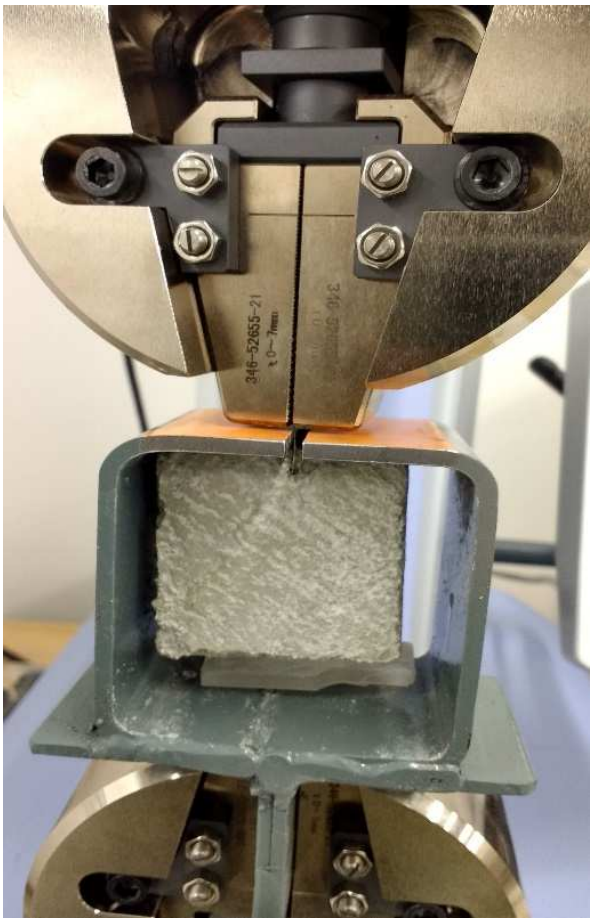

Figure 16. Peel test setup

Surface Roughness Tests

Steel and polypropylene fibers were required to determine their macro and micro profiles. Surface roughness is a physical property of fibers chosen as a variable in evaluation of the interfacial bond strength in new method. Though there were many surface roughness parameters available for measurement, the most commonly used R_a was chosen for this research study. These tests were conducted on KLA Tencor surface profilometer P-15 at the NDSU research park facility. The fiber specimens were cleaned using a blow dryer one night before the testing, and stored in air tight Ziploc bags to prevent any deposition of dust or moisture until testing. Although the research study focused on developing a relation between the surface roughness of the fibers and their bond strength in new method at a micromechanical level, specimens were tested for their

roughness and surface profiles at a macro level. There were three specimens each of steel, polypropylene, and wheat straw fibers for their macro profiles, and 25 specimens each for micro level surface roughness. The steel and polypropylene fibers used were obtained from manufacturing companies in a predesigned shape and size, which made it easier to study their macro profiles with few specimen tests and no loss of consistency. However, micro-level surface roughness is a parameter that needs to be statistically analyzed and so there were many more specimens tested for the same. As described earlier, these tests were performed on a surface profilometer working on a stylus measurement mechanism. The instrument contains a micro head at the bottom of the stylus (a needle like structure) with a radius of 25μm and an applied force of 2mg, initially focused and adjusted to touch the surface of the fiber specimen placed exactly under it. The stylus system has a microscope attached near the needle to record video during testing. Once the stylus was placed on the surface of the fiber, a scan length was inputted into the software system along which the stylus tip runs, measuring the peaks and valleys to produce a surface profile graph with measurement sensitivity up to angstroms.

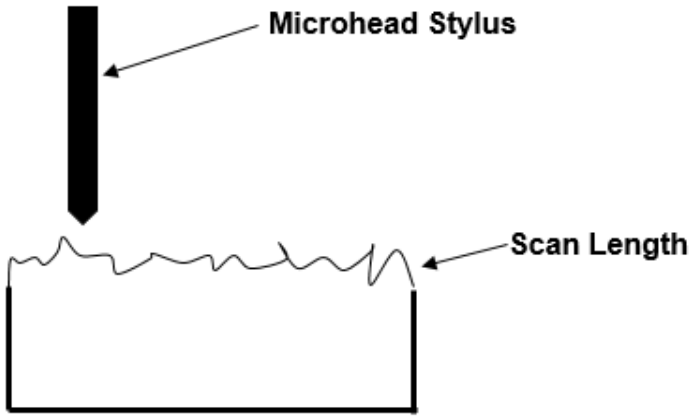

Figure 17. Working mechanism for surface profilometry

Surface parameters such as R_a, R_p, R_q, and RMS values were also evaluated and displayed by the software along with the profile. The data processing and acquisition was done through the computer connected to the surface profilometer. Macro profiles for steel, wheat, and polypropylene were developed by scanning specimens for a length of 10mm at a scan speed of 100µm/sec, with a vertical range/resolution for the stylus tip of 1048µm/0.6250A. There was one data point recorded for every 2µm of the scan length. For micro roughness profiling tests, vertical range/resolution for the microhead was set to 131µm/0.0781A for all the fibers. Scan lengths were set based on observations made from the macro profiles, 300µm for steel and wheat straw fibers, and 100µm for polypropylene fibers. After testing, raw data was exported in text format files to a jump drive. Further, analysis of raw data was performed to calculate the roughness parameters. The fiber specimens during testing were held onto a steel plate with tape to ensure that the axis of the fiber was perpendicular to the microhead's axis as shown in Figure 18.

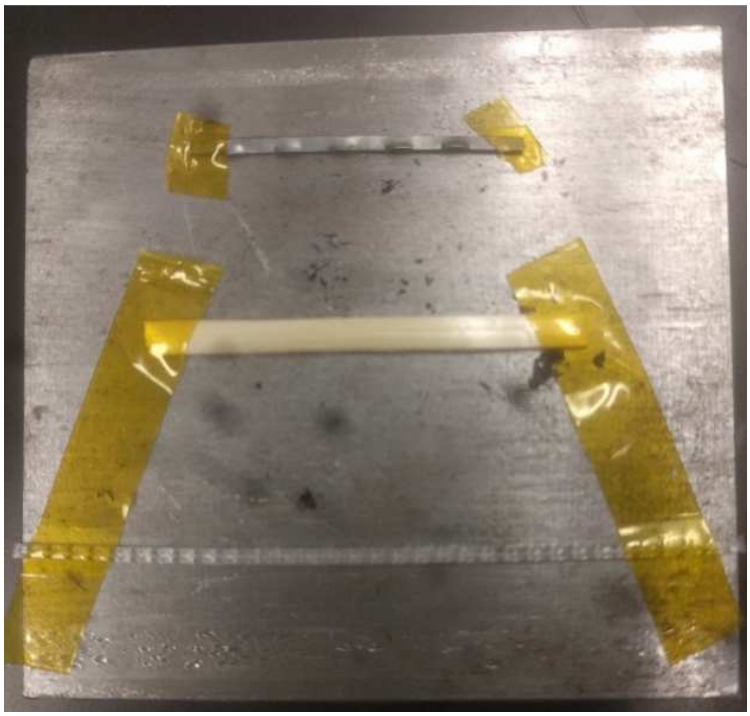

Figure 18. Test specimen for surface roughness

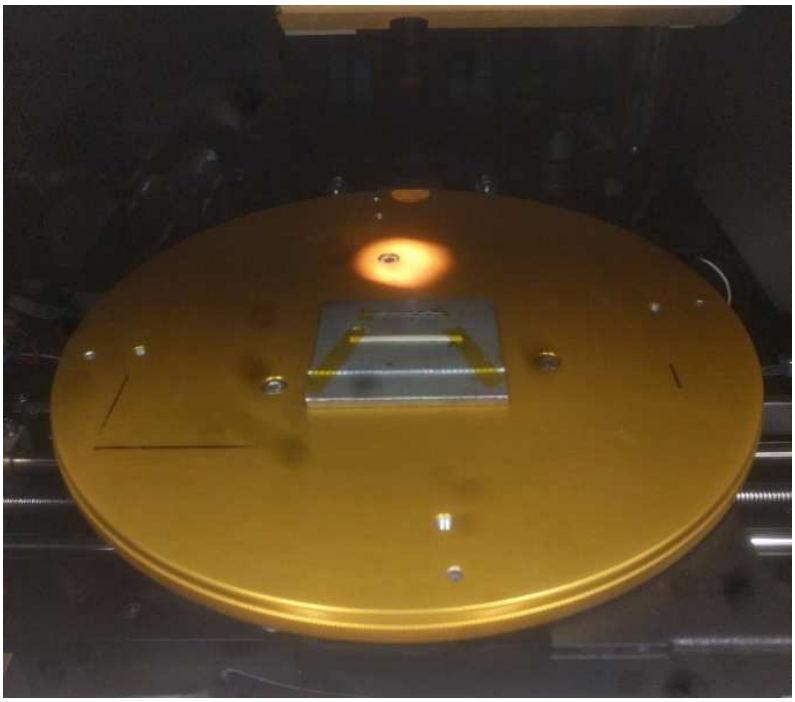

Figure 19. Test setup for profilometry

Compressive Strength Tests

For this research, Portland type 1 cement and sand were obtained from a concrete laboratory within the Department of Construction Management and Engineering at NDSU. Compressive strength was tested for this cementitious system as per ASTM code standards by casting 50mm cube specimens. The water-cement ratio was taken as 0.485, with proportions of cement, sand, and water for mixing mortar at 740g, 2035g, and 359ml for casting nine cubes as per ASTM C109M. These materials were mixed in a Hobart mixer according to the procedure described in C305 and the casted cubes were stored in a moist room for one day and then demolded to be transferred into a curing tank. The cubes were removed from the water tank after seven days, and checked for any irregularities on surfaces; any found were ground to smooth. The cubes were surface dried and placed on the bearing block in the compression testing machine which was calibrated, and the test ID saved for each specimen was tested. The load rate applied for compression was maintained in the range of 900N/s to 1800N/s as per the standard. While testing,

the load seemed to drop abruptly when the specimen failed. The test was then stopped then and peak load was recorded from the machine display. Later, the compressive strength was calculated from the formula $f_m = P/A$, where P is the load recorded, and A is loaded area surface. An average seven-day compressive strength of 35.5MPa was found for the mix used.

Tensile Tests

The fibers used in this research study were obtained from commercial fiber suppliers that provided standard peak tensile strengths for the fibers. However, elastic modulus values were not also provided by the suppliers, which necessitated performing tensile strength tests for steel and polypropylene fibers. These tests were conducted on MTS with a maximum load capacity of 5KN, provided with pneumatic grips. A load cell of 2KN was used for testing of the fibers and the crosshead displacement was set at 1.00mm/min. Ten specimens were tested for both steel and polypropylene fibers for their maximum tensile strength and elastic modulus and an average of these values was taken as their standard elastic modulus. The fibers were placed with approximately one third of their total length for tensile stress and elongation between the jaws. Pneumatic grips were tightened using an air pressure of 80psi for all specimens and the tensile strength and elastic modulus for wheat straw fiber were cited from previous research studies conducted by the Dr. Ravi's group. The MTS pull tester was connected to a computer for data acquisition.

RESULTS AND DISCUSSION

Modified Pullout Method

In this section, results for the new method were formulated in the tables and plotted in graphs for comparison purposes. After conducting experiments for the new method, raw data was exported from Bluehill, a data acquisition software for the Instron machine. The raw data obtained consisted of data points for extension and load for a corresponding time, and this data for all specimens was filtered and smoothened, using an exploratory data analysis which involved application of median filtering and smoothing through Hanning. There were eight specimens for each fiber type experimented on for the new method. Pullout curves were plotted for polypropylene fiber for embedment lengths of 10mm and 20mm in Figures 20, 21 respectively.

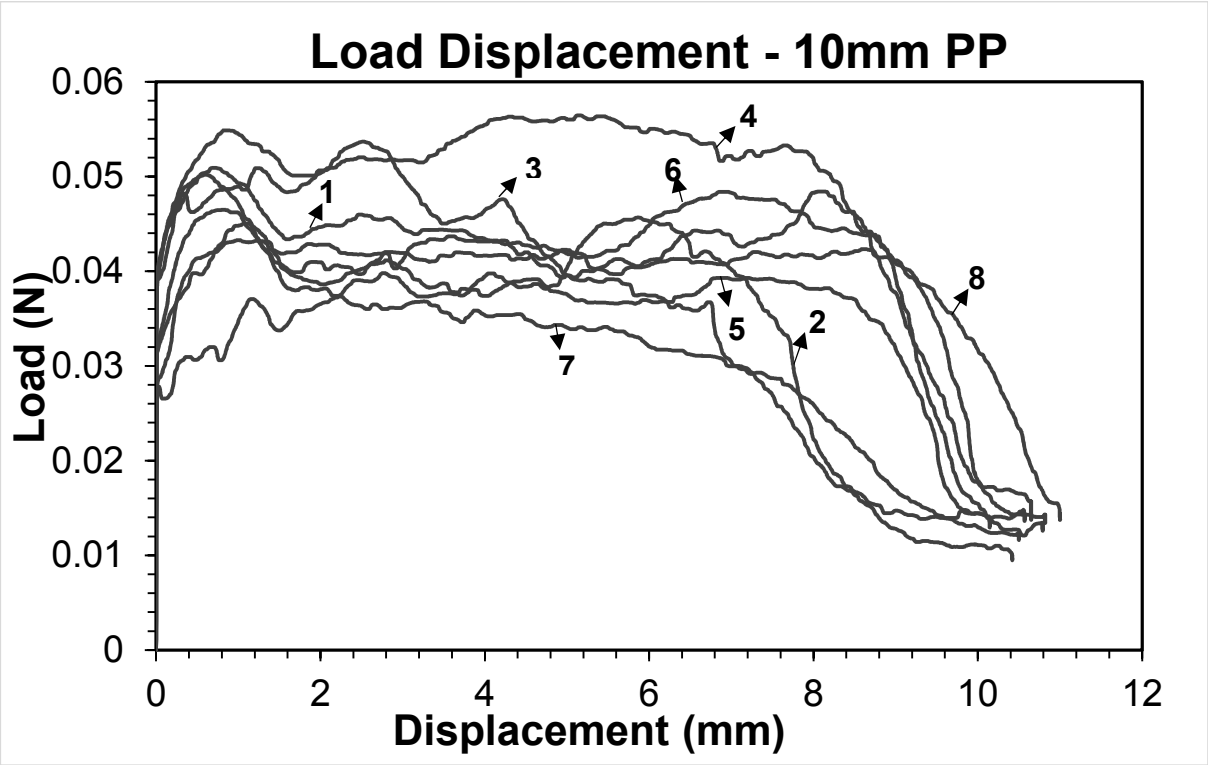

Figure 20. Pullout curves for polypropylene fibers for embedment length of 10mm

Since these curves are solely due to frictional interaction between the fiber and matrix, the peak load observed in pullout curves is considered the frictional load in this method.

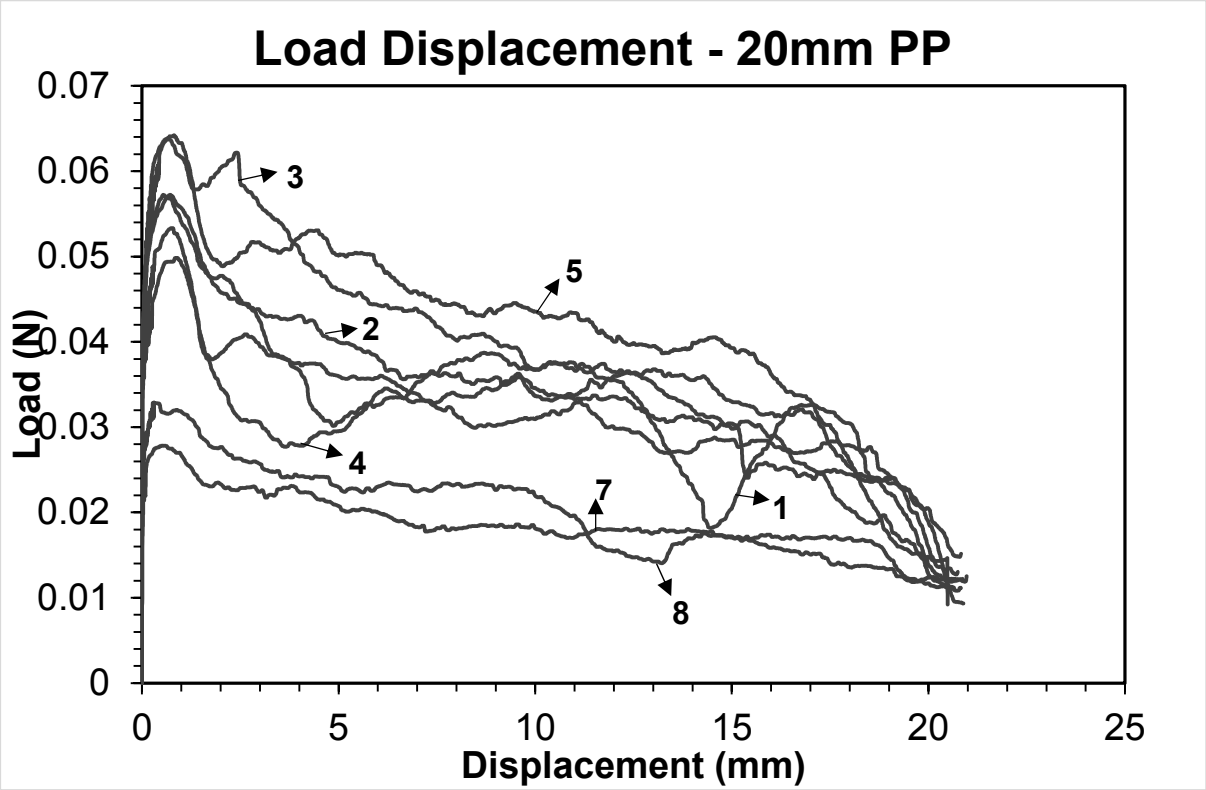

Figure 21. Pullout curves for polypropylene fibers for embedment length of 20mm

For the Figures 20 and 21, observe that with increasing embedment length for polypropylene fibers the pullout load range was increased. Also, 20mm embedment length for polypropylene test specimens has shown a higher variability in the pullout curves i.e., repeatability for polypropylene test specimens was higher for embedment length of 10mm. This will subsequently be explained as an effect of the fibers' surface roughness later. It was observed that the range of peak loads observed was from 30mN to 55mN approximately, and from 27mN to 65mN approximately for 10mm, and 20mm embedment lengths.

Load-displacement curves for steel fibers with embedment lengths of 10mm, and 20mm in cement-clay matrix were plotted in Figures 22 and 23 respectively. A different median filtering system was done for steel fiber pullout data as the raw data obtained showed high concentrations of noise.

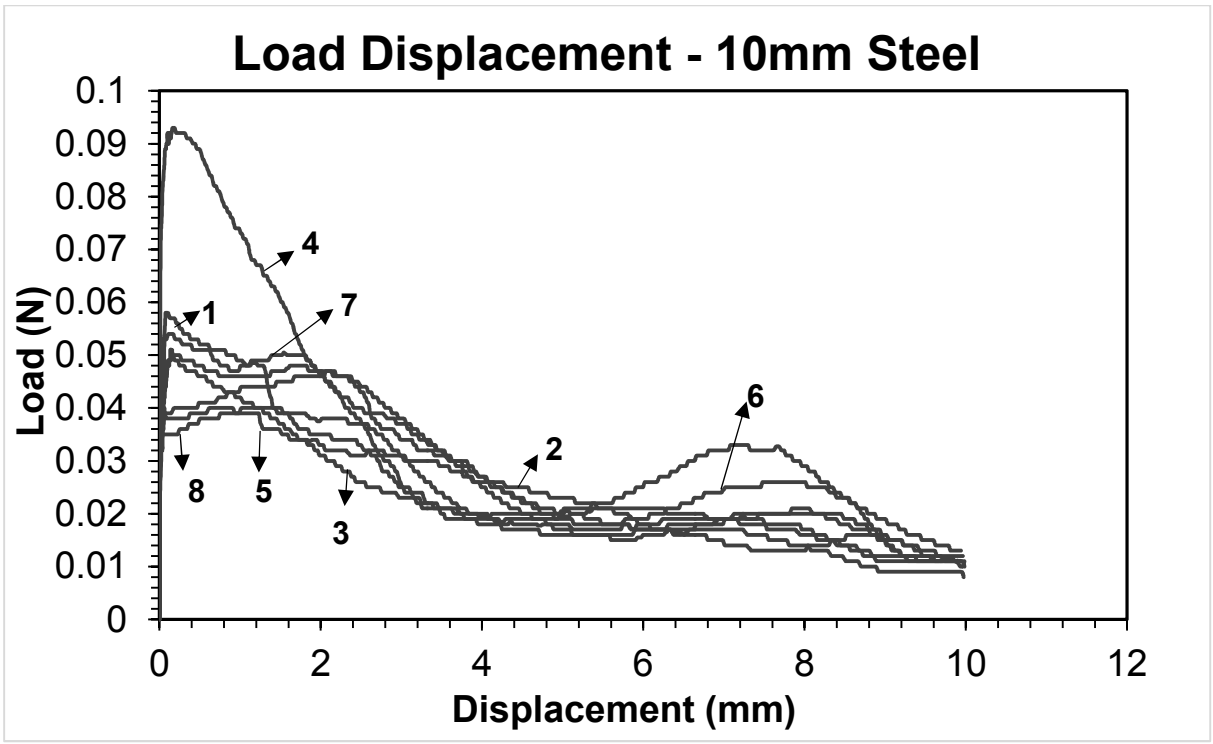

Figure 22. Pullout curves for steel fibers for embedment length of 10mm

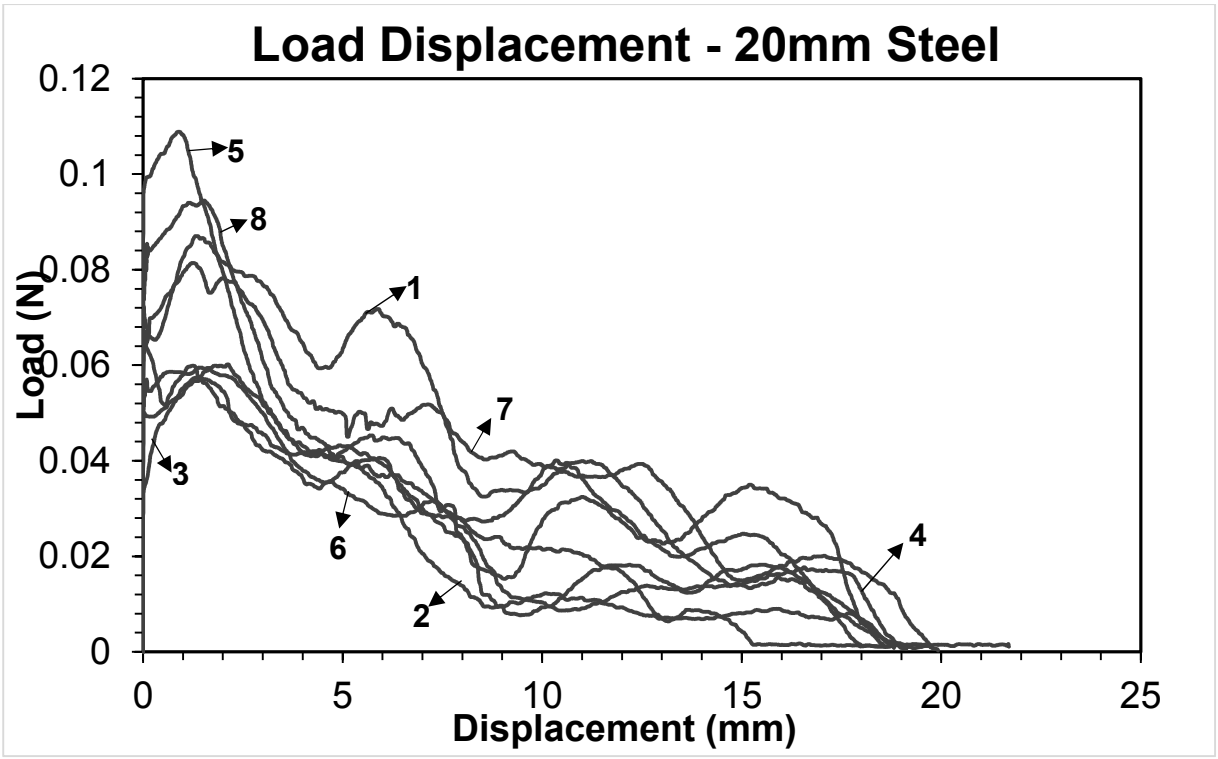

Figure 23. Pullout curves for steel fibers for embedment length of 20mm

Pullout curves for steel fibers have shown a higher range of peak pullout load for specimens when compared to previous results of polypropylene pullout curves. Specimen 4 in Figure 22 is clearly an outlier among the total eight specimens tested because of its very high peak pullout load. This can be explained by the inclination angle of the fiber in the matrix, where the orientation of fiber with matrix during pullout is explained in the literature. As such, there was not any unconventional pullout curve for the 20mm embedment length specimen set. However, the scatter among the peak pullout loads for 20mm embedded specimens is greater than that of 10mm embedment specimens. The surface profile of steel fibers was studied in detail later in the surface roughness section which explains the previous statement.

Load-displacement curves were plotted for 10mm, and 20mm embedment lengths of wheat straw fibers in the same cement-clay matrix in Figures 24 and 25 respectively.

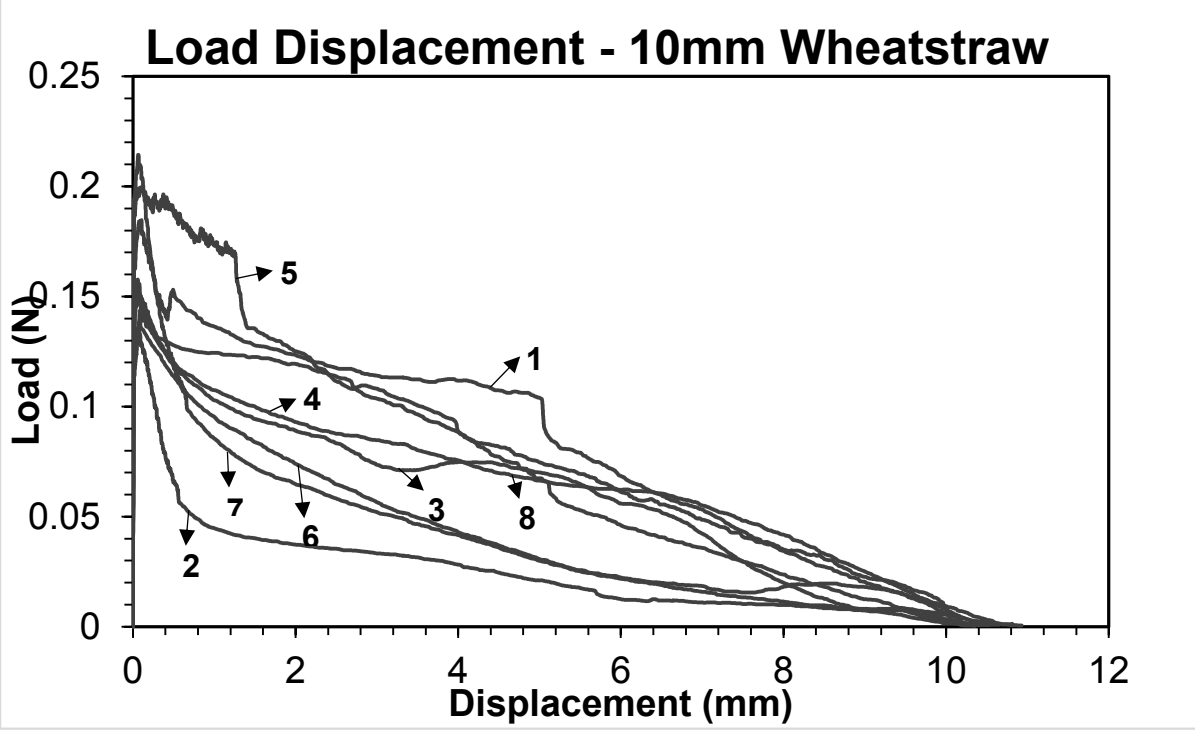

Figure 24. Pullout curves for wheat straw for embedment length of 10mm

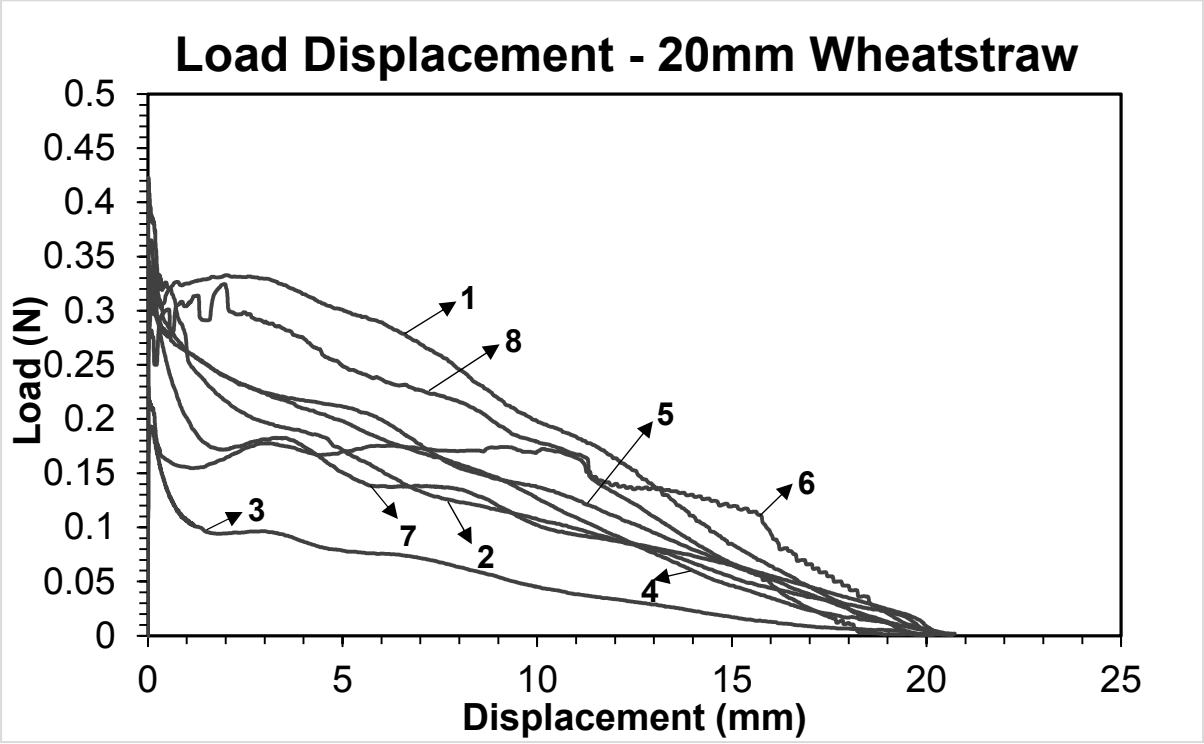

Figure 25. Pullout curves for wheat straw for embedment length of 20mm

Repeatability for wheat straw pullout curves as observed from the above figures is lower than what was observed for steel and polypropylene pullout curves. Since the wheat straw fibers have inconsistent surface characteristics, the variability in the peak pullout load was observed to be higher than design manufactured steel and polypropylene fibers. This will be discussed in the surface roughness section. The peak pullout load range for wheat straw fibers also increased with increase in embedment length. Specimens 1 and 5 in Figure 24, and specimen 8 in Figure 25 have shown sudden load drops in the pullout curves which indicated for slip in the fibers being pulled due to a probable zero friction between fiber and matrix.

Pullout parameters calculated from the plotted pullout curves for analyzing the fiber matrix bond behavior were peak pullout loads, pullout energies, and frictional bond strengths. Comparisons for pullout loads, pullout energies, and bond strengths were shown in Figures 26, 27

and 28 respectively. Note that a parameter comparison was done for the average values of eight specimens for each fiber type.

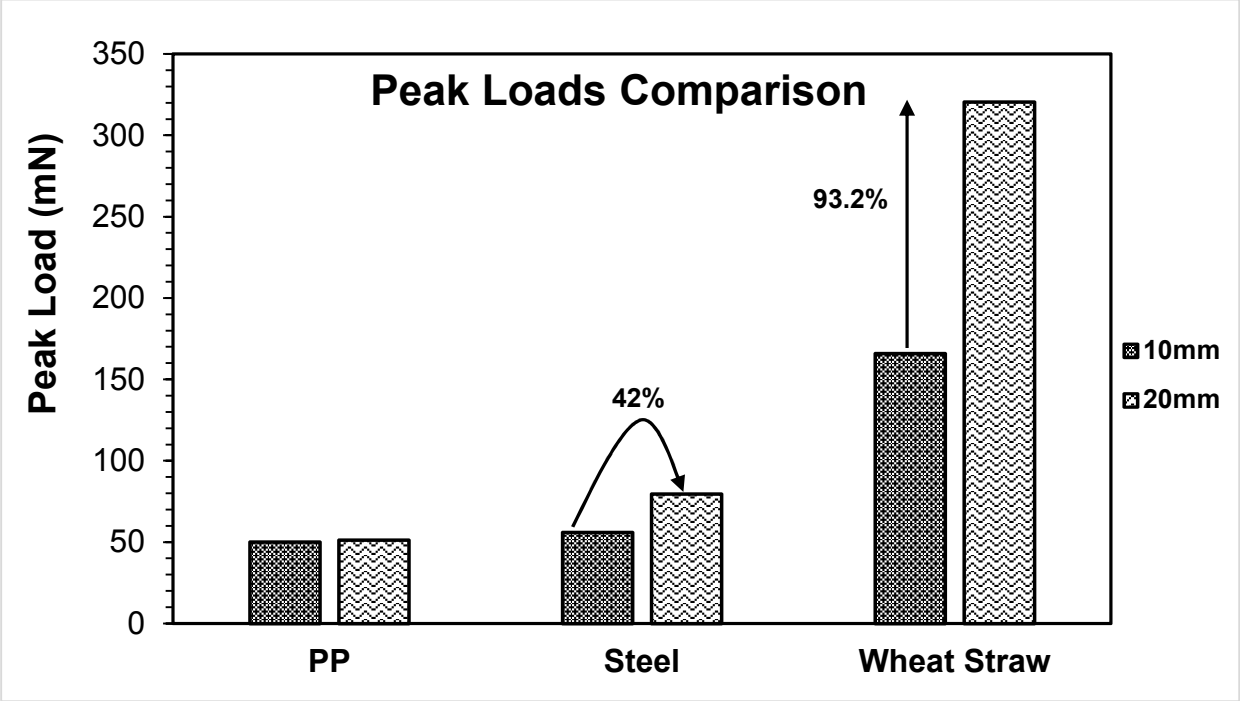

Figure 26. Pullout load comparison chart

Average peak pullout loads for polypropylene fibers were found to be 50mN and 51mN for embedment lengths of 10mm and 20mm, respectively. There was no significant increase in pullout load in this case. Whereas, steel fibers showed 42% increase in average peak pullout load from 56mN to 80mN for an embedment length increase of 100%. Similarly, for wheat straw fibers an average pullout load increase of 93.2% was observed from 166mN to 321mN for embedment lengths of 10mm and 20mm respectively. The comparison plot also indicates that wheat straw fibers exhibit the highest average pullout loads for the two embedment lengths of 10mm, and 20mm. The order of their peak pullout loads was observed to be wheat straw>steel>polypropylene, which indicates that wheat straw fibers have the highest capability in transferring load from matrix to fiber in pullout phase where the frictional bonding is the dominant mechanism.

From the load-displacement graphs plotted, average pullout energies for the curves were calculated and plotted in Figure 26. Pullout energy/pullout work performed was evaluated by calculating the area under curves (interpolation of the curves was done if needed) using the trapezoidal rule.

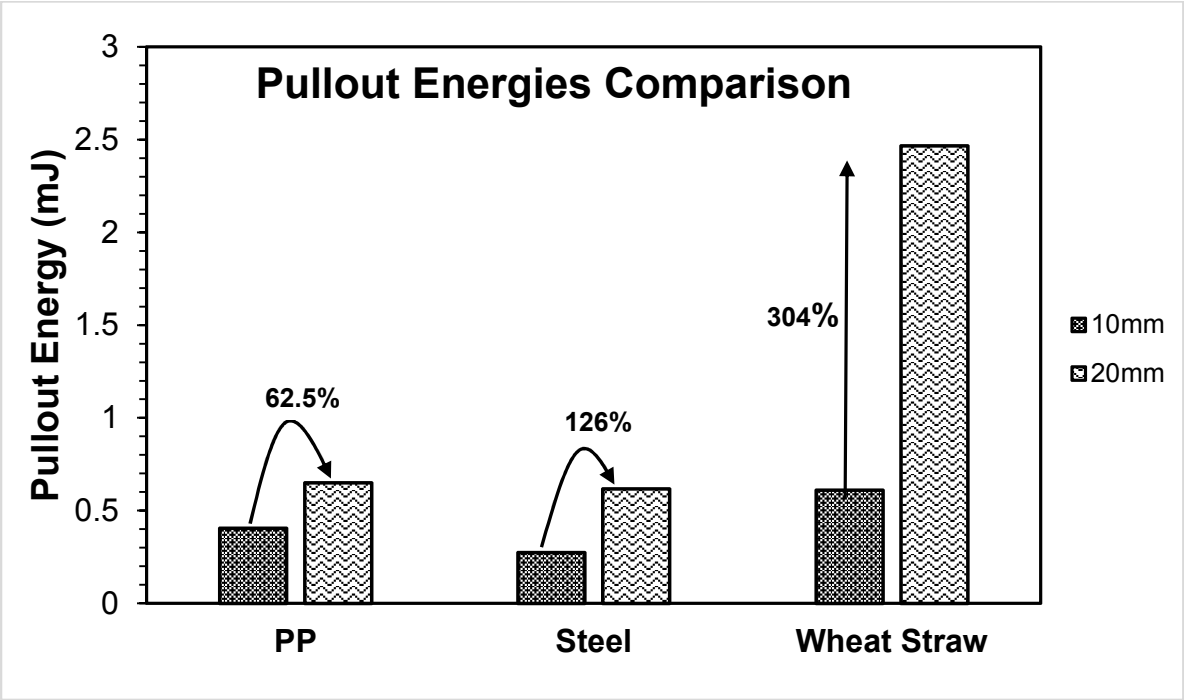

Figure 27. Pullout energies comparison chart

Pullout energy is the amount of energy required to pull the fiber out of matrix. High pullout energies signify high toughness in the composites and vice versa. In Figure 27, it was observed that the work performed to pull wheat straw fibers out of the cement clay matrix was significantly higher than that of polypropylene and steel fibers. Polypropylene fibers exhibited an average pullout work performed of 0.40mJ and 0.65mJ, for embedment lengths of 10mm and 20mm respectively. This indicated an increase of pullout work performed by 62.5% when the embedment length was increased by 100% (from 10mm to 20mm). Similarly, steel fibers reported average pullout energies of 0.274mJ and 0.62mJ, for embedment lengths of 10mm and 20mm respectively. The increase in pullout work performed for steel fibers associated with increase in embedment

length by 100% was found to be 126%. Average pullout energies observed for wheat Straw fibers for embedment lengths of 10mm and 20mm were 0.61mJ and 2.47mJ, respectively. There was an increase of 304% noticed in the case of wheat straw for an increase in embedment length of 100%. Results for the modified pullout method also indicate that for an embedment length of 10mm in the cement clay matrix, wheat straw fibers needed pullout energies of 51% and 123% more than what was needed for polypropylene and steel fibers, respectively. For an embedment length of 20mm, wheat fibers exhibited pullout energies of 279% and 300% greater than that of polypropylene and steel fibers respectively. Analysis from these results was made for wheat straw fibers showing high pullout energies for 20mm embedment length, indicating very high toughness of the composites in the post cracking stage for wheat straw cementitious composites.

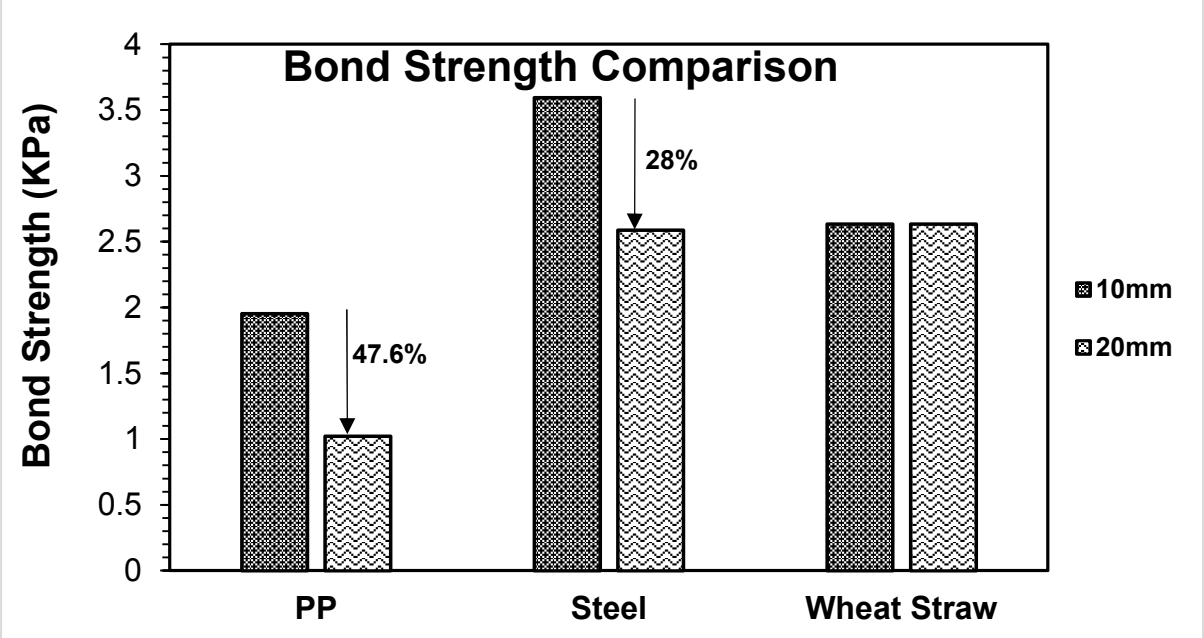

Figure 28. Interfacial bond strength comparison chart

Average interfacial bond strength of steel, polypropylene, and wheat straw fibers was evaluated using the formula, $\tau = P_{max}/(\pi d_f l_e)$ where τ is the average interfacial frictional bond

strength, P_{max} is the average of peak loads for all specimens for each fiber type, d_f is the diameter of fiber, and l_e is the embedment length of fiber in the matrix before the pullout.

Average interfacial bond strengths for fibers were found to be in the order steel>wheat straw>polypropylene for 10mm embedment length. Polypropylene fibers reported a least bond strength value for 20mm embedment length as well, while the other two fibers steel and wheat straw exhibited almost equal bond strength values. Comparison of the bond strength values between two embedment lengths for a fiber reported a different behavior as observed in their peak loads graph. A decrease in bond strength of 47.6% from 1.95Kpa to 1.022KPa was noticed in case of polypropylene fibers with an increase in their embedment length from 10mm to 20mm. Steel fibers showed a decrease of 28% bond strength from 3.59KPa to 2.58KPa for an increase in their embedment length by 100%. Interestingly, wheat straw fibers showed almost equal bond strength values for both embedment lengths, which indicates that their interfacial bond strength is independent of the embedment length. The order of their bond strengths is explained next in surface roughness section.

Surface Roughness Tests

This research study was conducted to establish a relation between the surface roughness of the fibers and the frictional bond strength reported in the modified pullout method proposed. Materials surface characteristics can be broadly classified into two types and when the surface profile is analyzed for a certain span, there are two different characteristics namely waviness and roughness (Vorburger & Raja, 1990). Macro-level surface pattern is characterized by the waviness factor of a material, while roughness is the parameter for studying the detailed micro-level surface characteristics. The interfacial bond study in the current study being a micromechanical analysis, roughness of fibers was investigated. The raw data collected from KLA Tencor profilometer's

software was processed to evaluate the arithmetical mean roughness index (R_a) for fibers. Columns with number of data points, corresponding profile values, and leveled profile values were acquired from the profilometer's software. These data points when plotted in Excel give the profile for the scanned length of the material. The profile is divided into two regions of equal areas by introducing a mean profile line in the scan profile curve. The perpendicular distance of the points on the profile curve from the mean line were calculated, and an average was taken to produce the final arithmetical surface roughness index in microns as shown in Figure 29.

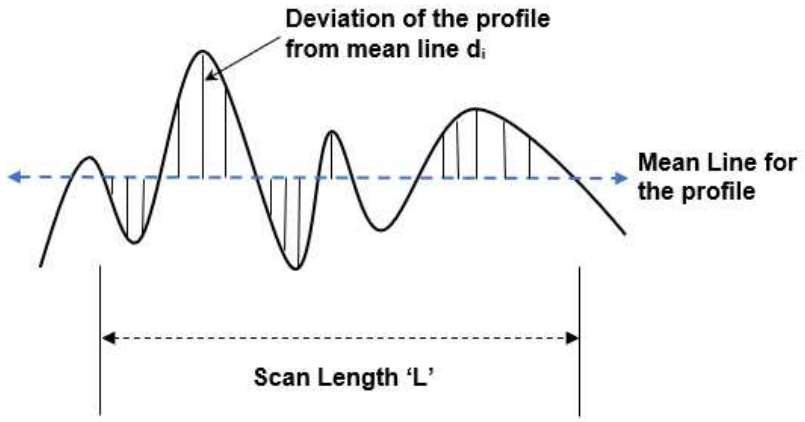

Figure 29. Schematic description for surface profiles

Roughness of the profile in the above drawn figure where the deviations of the z-axis data values from the mean line were denoted as d_i is calculated from the formula, $R_a = \frac{\sum|d_i|}{n}$, where n is the number of data points recorded in scan length L.

There were 25 specimens tested for each fiber type in this test as mentioned in the methodology chapter earlier. There was one scan length of 300µm each measured on each specimen for steel and wheat straw, while the specimens of polypropylene were measured for 100µm due to their repetitive curvature for intervals at every 150-200µm, posing a challenge for

scan length to go beyond the lower limit. Scatter plots were developed for each fiber type in the following figures.

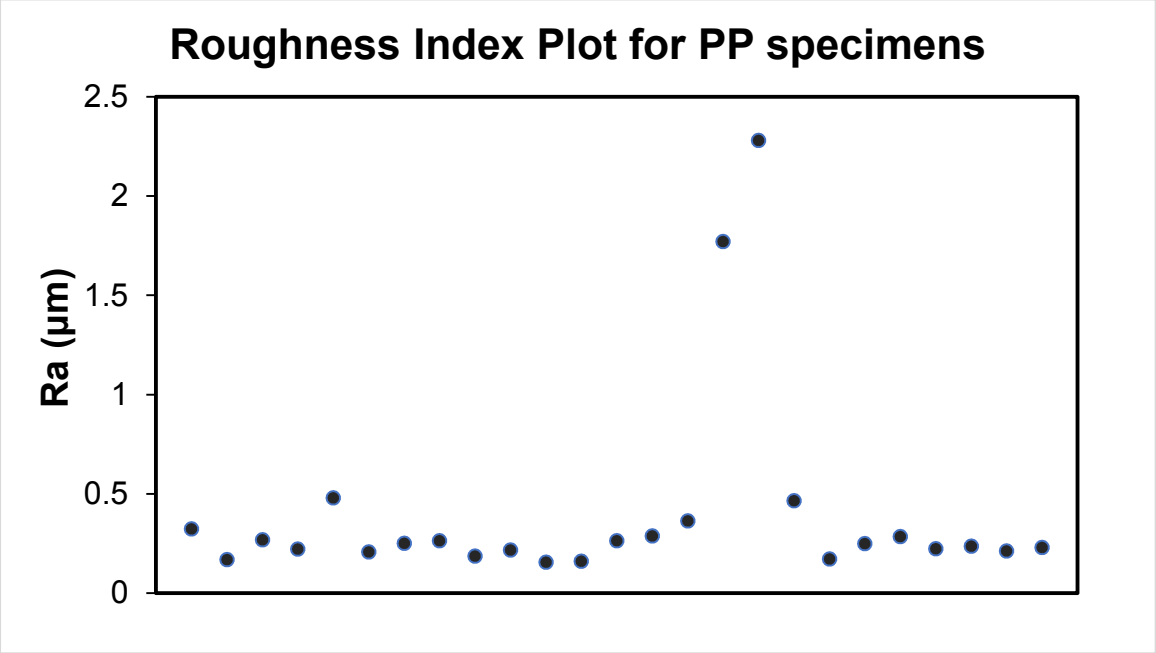

Figure 30. Roughness scatter plot for polypropylene fibers

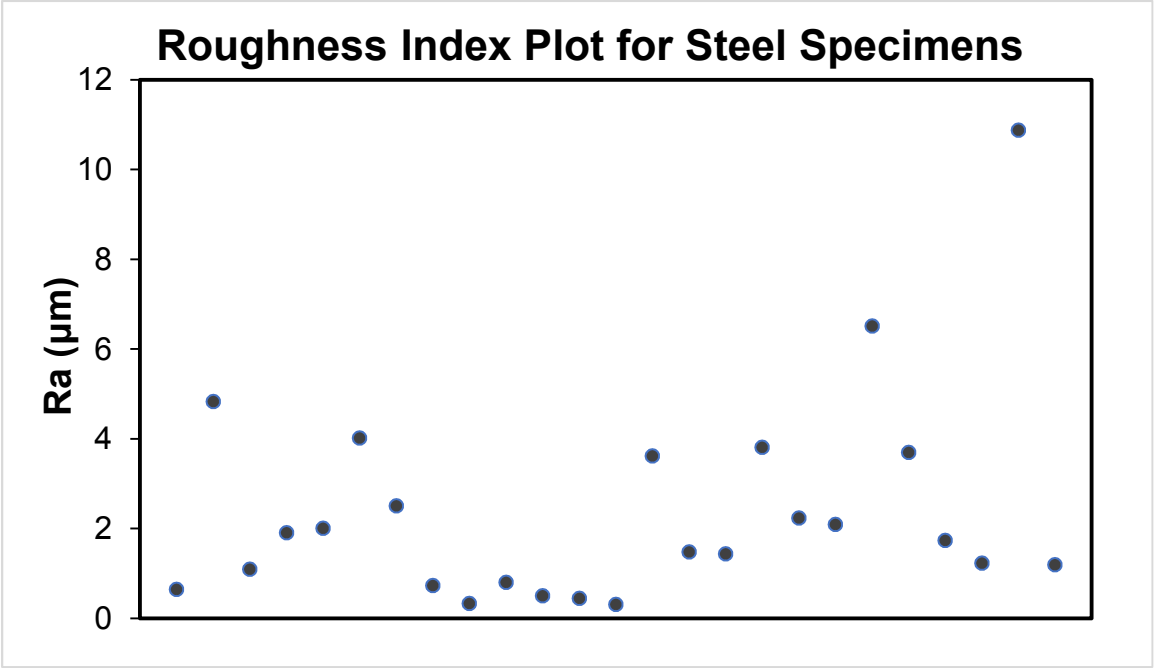

Figure 31. Roughness scatter plot for steel fibers

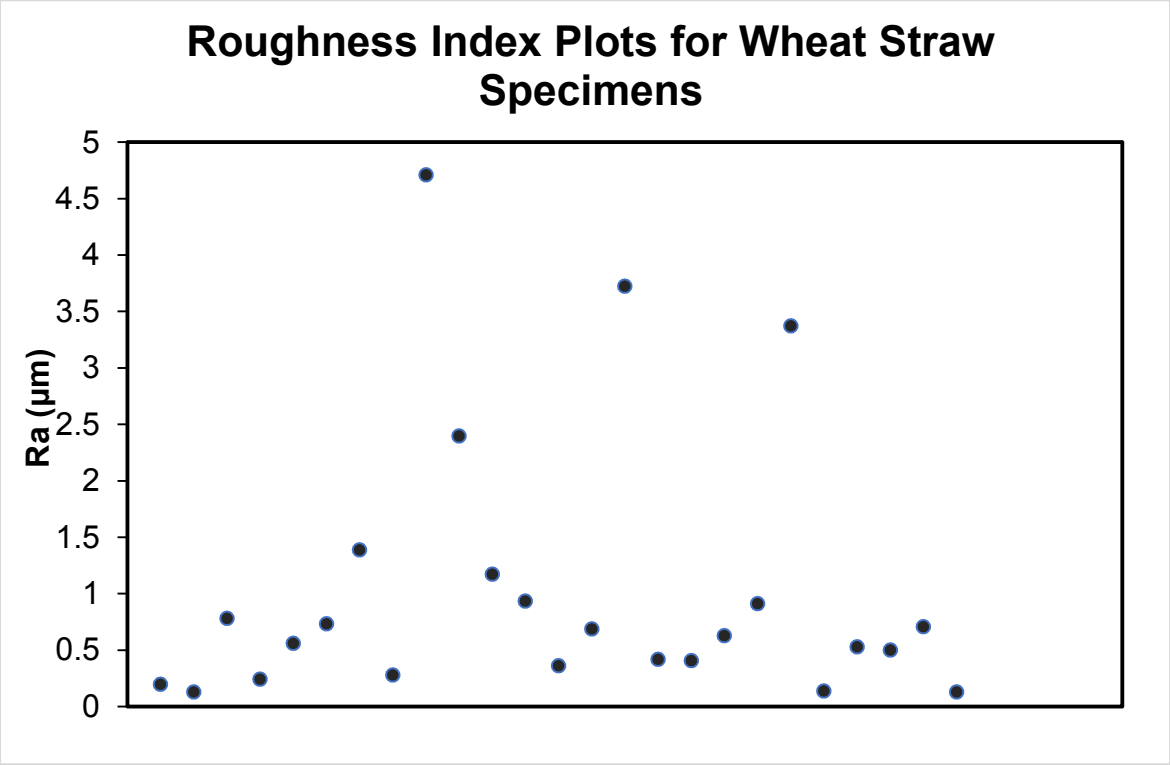

Figure 32. Roughness scatter plot for wheat straw fibers

The scatter plots give an outline of random distribution for surface roughness indices for each fiber type. Polypropylene fibers in figure 30 have exhibited consistency better than steel and wheat straw fibers for roughness values. The nature of polypropylene fibers derives from polymer resins that maneuver consistency factors for their physical structure. However, there were outliers noted in the polypropylene fibers scatter plots, exhibiting high roughness indices from their average value. Steel fibers have shown greater scatter in their distribution owing to the very innate nature of the material manufacturing and have displayed more than a couple outliers in the scatter owing to at least 10% chance of uneven surface characteristics in a set of 25 specimens. Wheat straw being natural fibers has exhibited the highest variability in the roughness scatter as expected owing to their inconsistent surface characteristics. There is at least 20% chance of producing fibers with an outlying roughness index when compared to the average value in a set of 25 test specimens. The roughness index variability has shown to increase in the order polypropylene<steel<wheat

straw for a set of specimens tested. Hence, an expected order of probability distribution has been observed due to the natural fiber's uneven and inconsistent surface characteristics, as reported in previous research studies.

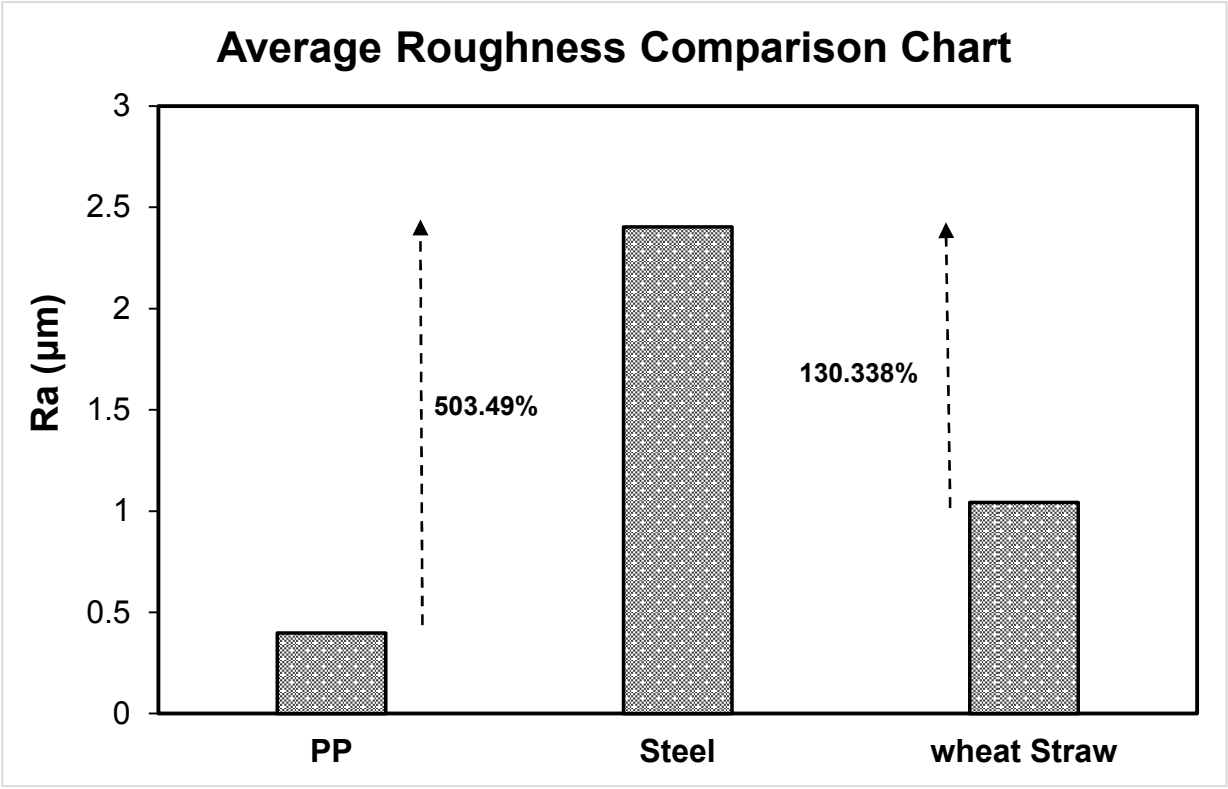

Figure 33. Average roughness comparison chart

The average surface roughness indices for each fiber were evaluated and plotted for a comparison analysis in the Figure 33. The order of their surface roughness indices was observed to be in the order of their bond strengths in new method i.e., steel>wheat straw>polypropylene. Steel fibers have exhibited the highest surface roughness index at about 503.5% and 130.34% higher than that for polypropylene and wheat straw fibers. Figures 28 and 33 provide a validation for the modified pullout method proposed where it was proven that a higher interfacial frictional bond strength is obtained for a fiber with higher surface roughness. Hence, it can be stated that higher surface roughness index for a fiber provides a better mechanical interaction with the matrix.

Standard Pullout Test Results

Conventional single fiber pullout tests were conducted to verify the modified pullout method proposed. This section provides the results of standard pullout tests for polypropylene and steel fibers embedded for a single length of 10mm in Portland type 1 cement mortar mix. Seven mortar cubes of both steel and polypropylene fibers were cured for seven days post mixing and were tested for pullout. Noise reduction for the raw data was done using median filtering and Hanning, which provided the final data for plotting curves. Figures 34 and 35 depict the pullout load vs displacement curves for polypropylene, and steel fibers for an embedment length of 10mm. Average peak loads and pullout energies for the seven specimens were calculated from the filtered data for polypropylene and steel fibers and then were compared as shown in Figures 36 and 37.

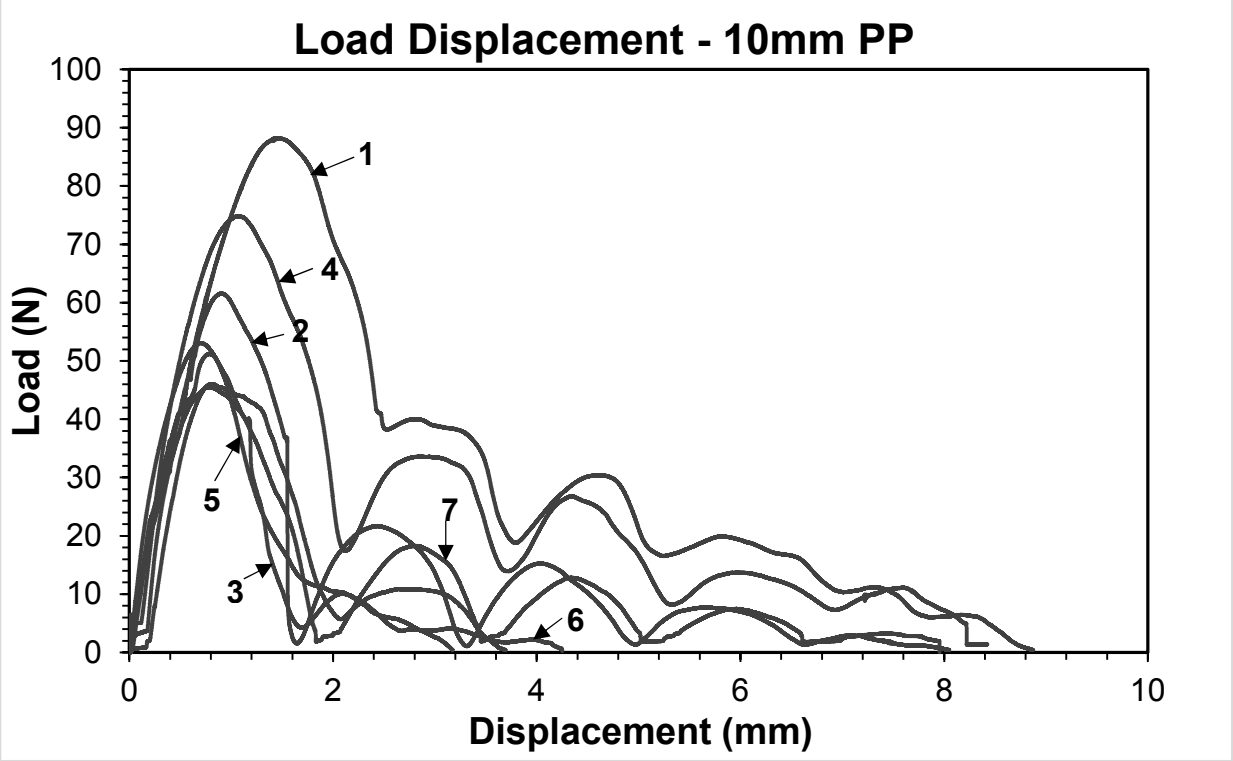

Figure 34. Standard pullout curves for polypropylene fibers

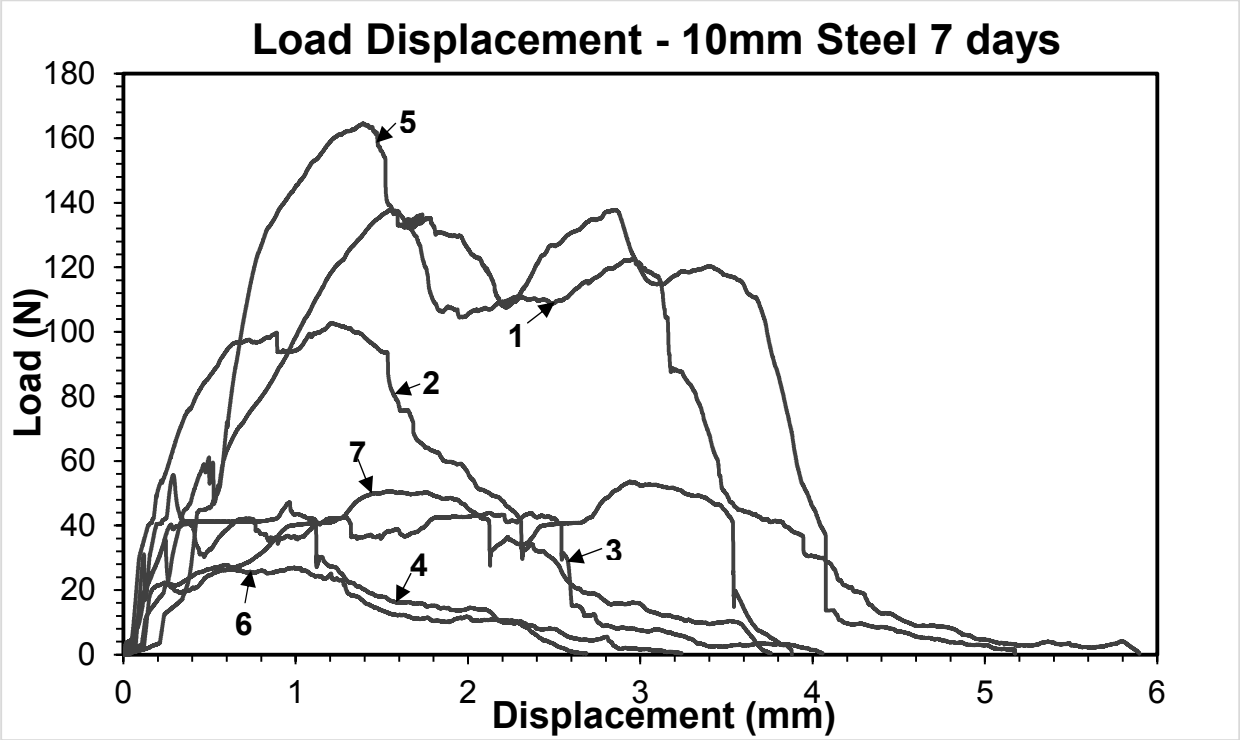

Figure 35. Standard pullout curves for steel fibers

Pullout for polypropylene fibers show a better repeatability than steel fibers as observed from their load-displacement curves. Inconsistency in the pullout curves can be attributed to the heterogeneity of the matrix's chemical characteristics i.e., mortar cubes prepared for a particular fiber test specimen have different elastic bonds. Variability in the pullout load range is very high for steel fibers at a difference in the least and maximum pullout loads recorded of 140N, when compared to a 40N difference for the range of peak pullout loads in polypropylene fibers. The maximum displacements of steel fibers in pullout curves was observed to be 6 mm, a relatively lower value compared to that of 8mm in polypropylene fibers curves. This indicates that the pullout phase of steel ends earlier than it was supposed to, due to a depleted mechanical interaction at the interface. Conventional pullout curves have reported for both chemical and frictional bond phases involved in the analytical models are mentioned in the literature section. The typical pullout curves in this research for standard single fiber pullout tests were explained by considering a single

representative curve for the set of seven specimens with reference to (Katz & Li, A special technique for determining the bond strength of micro-fibers in cement matrix by pullout method, 1996) model.

Typical Pullout Curve Analysis for Single Fiber Pullout Tests

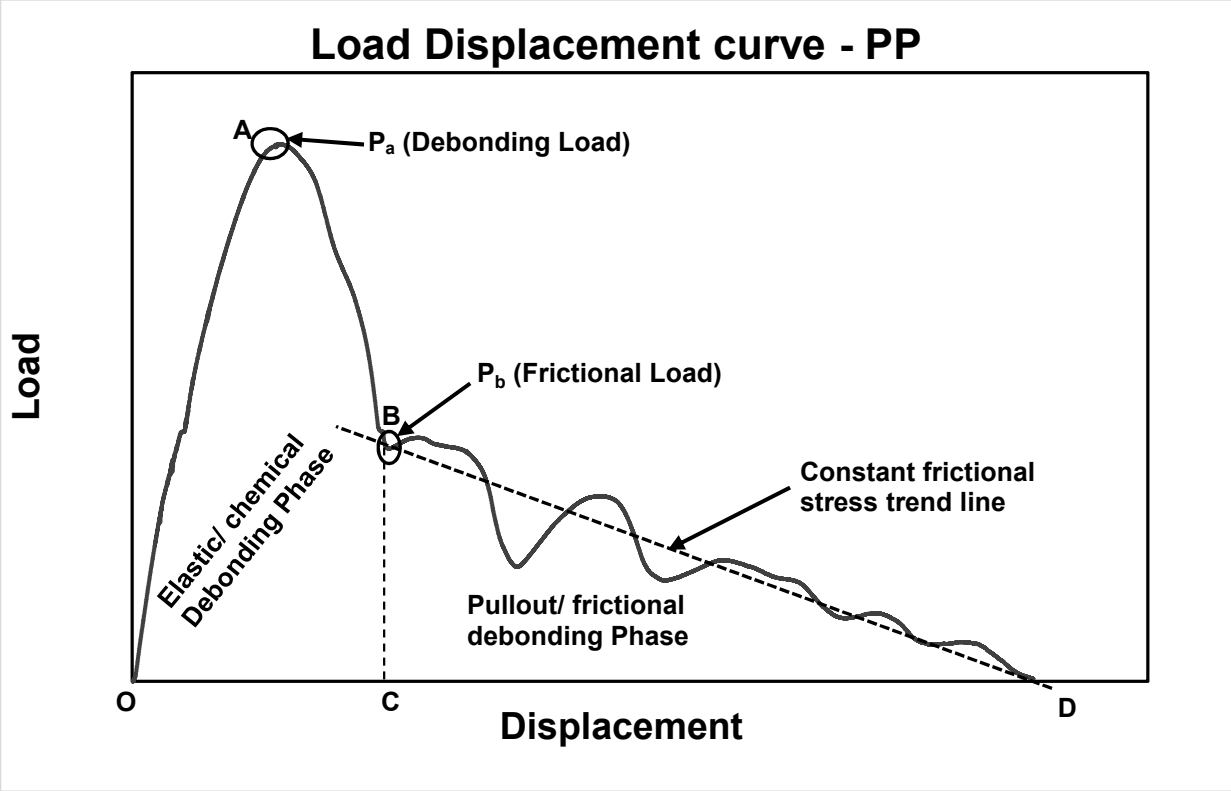

Figure 36. Typical bond-slip mechanism for polypropylene pullout curves

The above shown figure represents the typical single fiber pullout curve for the set of individual load displacement curves for seven days cured polypropylene pullout specimens with an embedment length of 10mm. As shown in the Figure 36, the pullout mechanism is comprised of two different activities occurring in sequence. When the pullout experimentation starts, the fiber shows an almost linear increase from O to A during which the partial debonding takes place i.e., the curve OA represents the chemical/adhesive debonding and hence the high load recorded for a very short slip in the bond. Further the peak debonding load is reached at P_a where the chemical bond is lost, and the fiber starts slipping without any resistance for a short slip from A to B until

complete elastic debonding takes place. AB represents the final elastic debonding curve after which the load-slip behavior of the fiber was observed to be non-linear. This can be explained by the fact that during the pullout process from A to B, the fiber supposedly has some surface roughness and abrades the surrounding matrix material due to which the fiber-matrix interface develops some frictional interaction. Even more, there might be added frictional resistance from the abraded particles of the medium or fiber when they fall in the pullout cavity, and due to which there might be a slip-hardening effect seen. Area under the curves OAB, and BD gives the amount of work done for chemical/elastic debonding and frictional debonding phases. Area of OABC gives the debonding energy needed for complete elastic debonding of the fiber matrix interface, while area of BCD gives the pullout energy needed for the pullout of fiber from the matrix. Also, to determine if there is slip-hardening effect, a straight line was drawn from the point B to D which gives a hypothetical formulation for a constant frictional bond slip. The area under the triangle BCD gives the pullout energy offered by frictional force for a constant bond-slip and the difference between the area under curve BCD and the triangle BCD gives a very minimal value, but does not imply constant frictional stress during the pullout phase. For the polypropylene curve shown in Figure 1, the percentage difference between areas of curve under BCD and triangle BCD is very minimal which might mislead into assuming an absence of slip-hardening effect. But, the pullout phase through BD has a couple of dips before it attains an almost linearity. The dip in the curve signifies the slip-softening followed by a slip-hardening effect. The steel fibers used in this research study were deformed/ crimped. Undulations on the fiber have been studied using profilometry and the macro-profiles for the same were reported in the appendix. Deformed steel fibers have shown a variable slip during the pullout tests as reported in the literature.

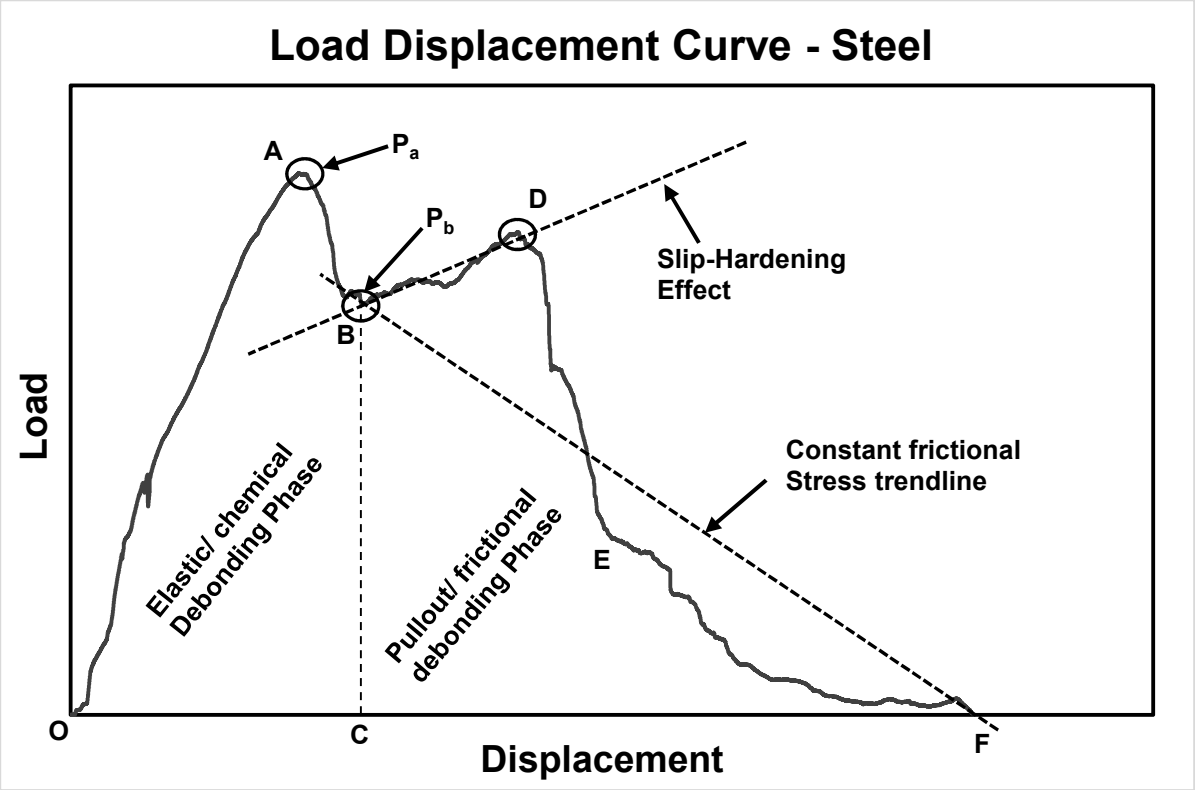

Figure 37. Typical bond-slip mechanism for steel pullout curves

A similar bond-slip theory is used to analyze the typical curve for steel fiber as shown in Figure 37. Curves OA, AB, BF represent partial debonding phase, complete debonding phase, and pullout phase respectively in the graph. The debonding behavior for steel fiber was partly similar to that of polypropylene fiber, where it showed an almost linear behavior for load-slip relation from O to A to reach the peak debonding load, before dropping at a linear bond-slip rate from A to B to attain the complete loss of adhesive bond in the fiber-matrix system. The load recorded at this point B was the pure frictional force acting at the fiber-matrix interface. An observation made in the pullout phase for a steel fiber typical pullout curve was, that the curve BD part refers to increasing frictional stress for a part of slip and hence a major slip-hardening effect was seen along the line BD, and then slip dropping linearly until the point E for a constant frictional bond stress, followed by a slip softening effect from E to F where the frictional bond stress decreases gradually. Usually, a constant frictional bond stress line drawn gives an idea of any slip- hardening and slip-

softening effects present in the pullout behavior of the fiber matrix system. The consecutive slip-hardening and slip-softening effects in the pullout phase have shown an equal amount of pullout energy calculated for the actual curve against the hypothetical curve with constant frictional stress. In simpler words, the area under curve BF and the area of triangle BCF produced close values.

Pullout Parameters and Their Comparison

From these curves, the peak debonding loads and peak frictional loads for all were noted and averaged to evaluate average debonding load and average frictional load for steel and polypropylene fibers, as compared in Figure 38. Similarly, the energies associated with debonding and pullout as earlier explained in the typical curve mechanism were calculated by evaluating the areas under corresponding curve sections for all the specimens, then averaged and plotted in the Figure 38. Comparison figures depict 2-D column stacked charts that give an understanding of peak loads and total energies as part of the whole entity for both fiber types.

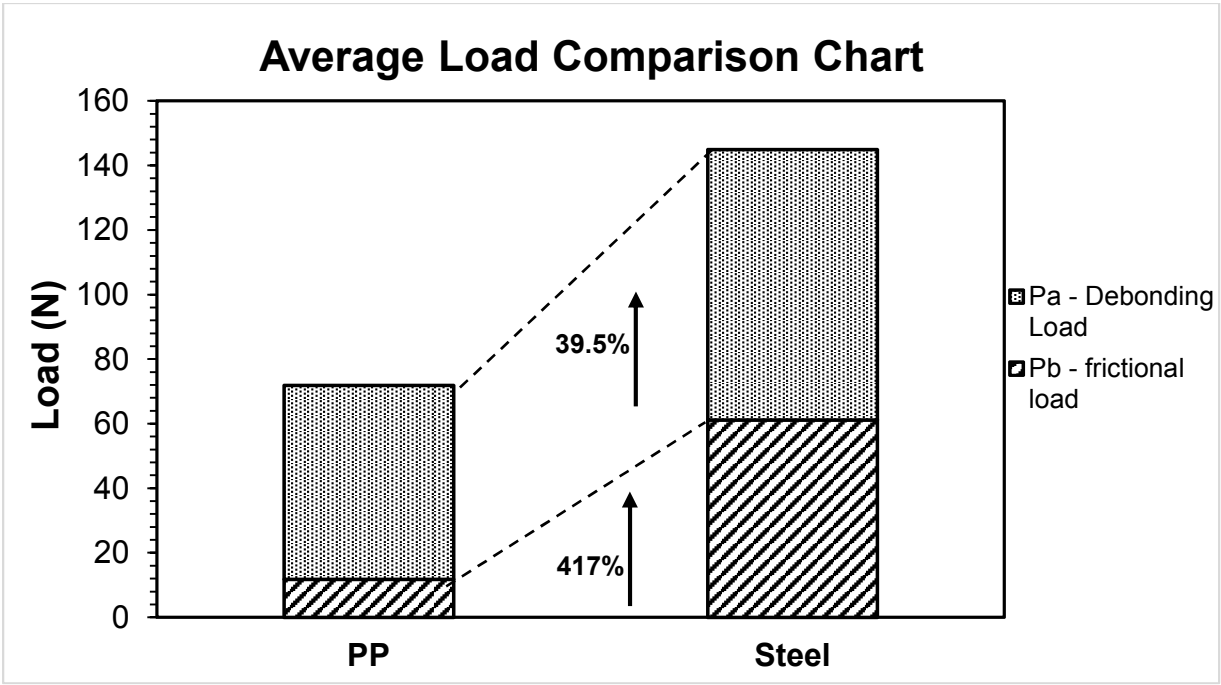

Figure 38. Average load comparison chart

Steel fibers at 83.78N exhibited a higher average debond load recorded by 39.5% than that of polypropylene fibers at 60.06N, which indicates that the load transfer during the pre-cracking stage is higher for steel fibers. This can be attributed to their high elastic modulus compared to that of bundled polypropylene fiber in this study. Average frictional load for steel fibers at 61.208N was greater than polypropylene fibers at 11.837N by a staggering value of 417%. The relatively high value of frictional load for steel characterizes the capability of the interface for a steel-cementitious system in transferring load from matrix to fiber during the post-cracking stage. This can be attributed to the higher peak tensile strength of steel fibers compared to polypropylene.

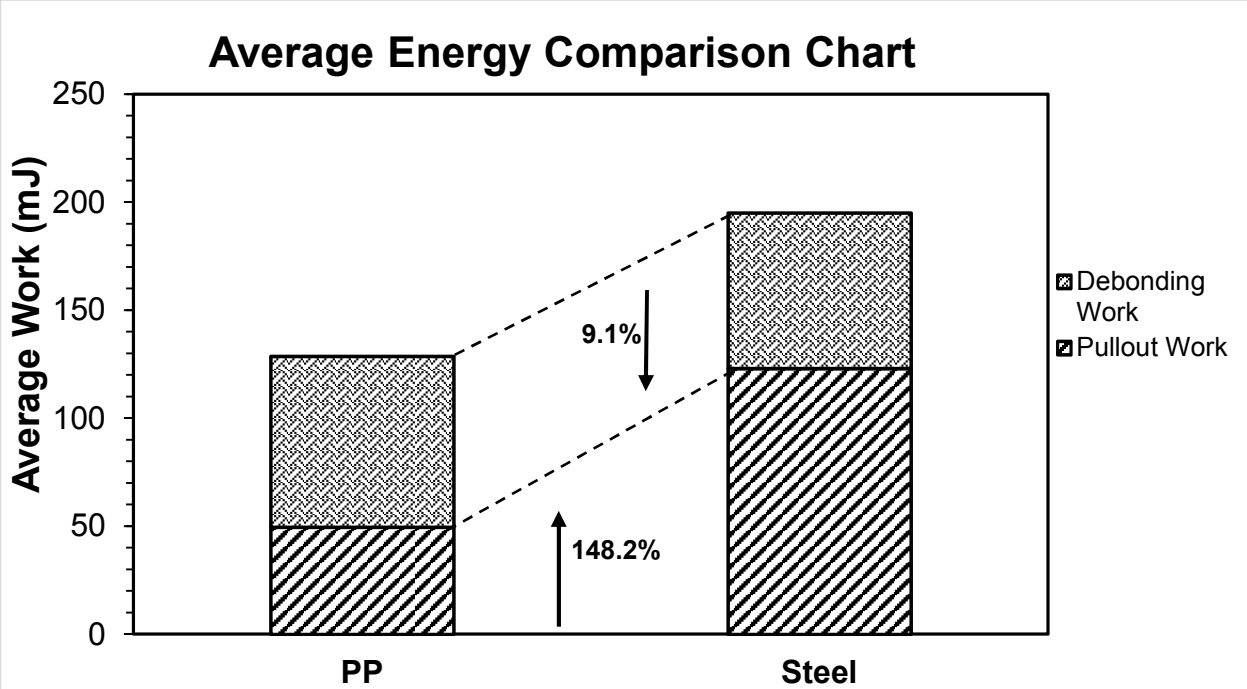

Figure 39. Average energy comparison chart

Average total energy consumed during the pullout process, and average peak load throughout the process for polypropylene fibers were observed to be higher than steel fibers. Average total energy values for polypropylene and steel fibers were 128.71mJ and 195mJ. The average debonding energy, and average pullout energy consumed constituted to 61.5%, and 38.5% of the total energy consumed for polypropylene fibers pullout curves respectively. Similar

observation made for steel fibers indicated the total energy consumption comprising 36.9% energy during debonding phase, and 63.1% during pullout phase. The energy chart indicates that the average debonding energy consumed during the debonding phase was higher for polypropylene than steel fibers by 9.1%. Contrary to the earlier made observation, steel fibers demonstrated an average pullout energy consumed during pullout phase (post-debonding) greater than that of polypropylene fibers by a remarkable value of 148.2%. The reported higher energy values of steel fibers in the pullout phase signify the toughness in steel-cementitious composite during the post-cracking stage.

Interfacial frictional bond strength is calculated by using the equation, $\tau_0 = \frac{P_b}{\pi d_f l_e}$, where P_b is the peak frictional load, d_f is the diameter of fiber, and l_e is the embedment length (Leung and Li, 1995).

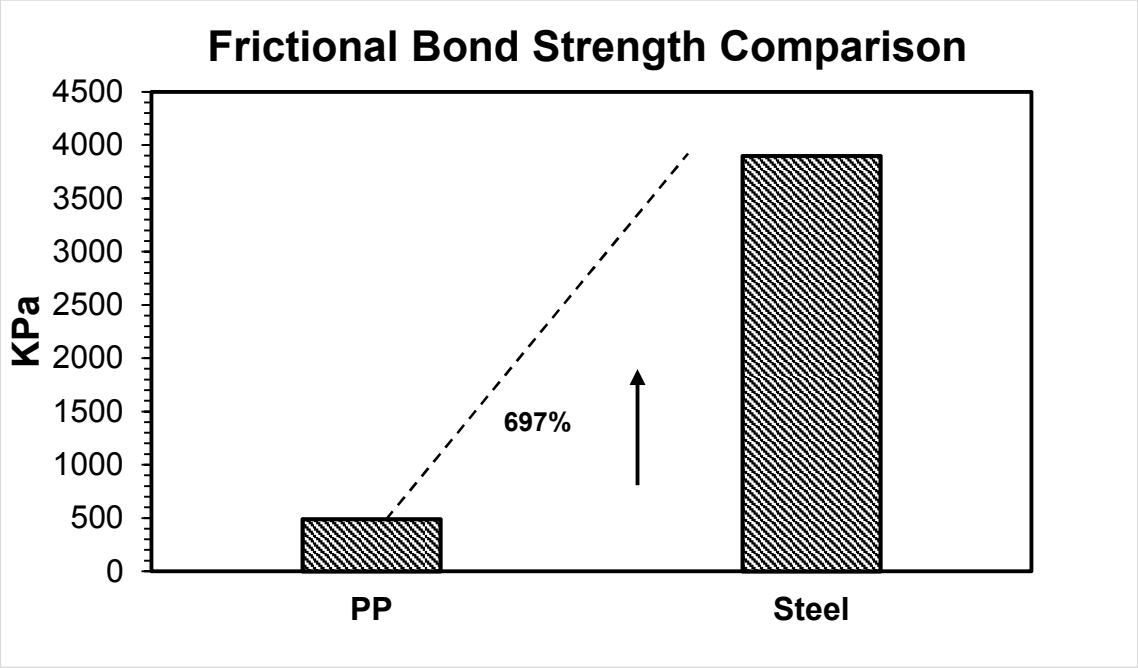

Figure 40. Frictional bond strength comparison chart

Polypropylene fibers reported an average frictional bond strength of 490KPa when compared to that of steel fibers at 3900KPa. Steel fibers which have reported a higher pullout work

performed and higher frictional loads exhibited the same behavior in case of bond strength values as well. The average bond strength due to the friction between the steel fibers and the cementitious matrix was observed to be 697% greater than that of polypropylene fibers. Difference in the bond strength values of the steel and polypropylene fibers were observed to be in the range of the percentage difference of their average frictional load values. Another observation that was made from the pullout results analysis was that the average values of pullout energy, pullout load, and bond strength were reported to be higher for steel fibers than those of polypropylene fibers. The high frictional bond strength of steel fibers can be attributed to their surface roughness, and their mechanical interaction with matrix was explained in SEM and EDS analysis in the next section.

Scanning Electron Microscopy (SEM) and Energy Dispersive Spectroscopy (EDS) Analysis

This section discusses the qualitative analysis of scanning electron microscopy images in conjunction with energy dispersive spectroscopy images of fibers pulled from cementitious matrices in single fiber pullout tests. Scanning electron microscopy (SEM) analysis of the pulled-out fibers characterize the bonding of the fibers in pullout tests qualitatively in both chemical, and frictional debonding phases. However, the inferences made from SEM images for the deposited materials on the surface of fibers need to be accounted. Hence, the pulled-out fibers were analyzed with Energy Dispersive Spectroscopy (EDS) testing to quantify the chemical depositions on the fibers. The following images depict the EDS analyzed Back Electron Scatter (BES) images of pulled out steel and polypropylene fibers. There was one pulled out fiber each for steel and polypropylene that was analyzed with SEM, with 10 random shots taken from different magnification levels, but only representative results were discussed in this section. The BES images were analyzed at more than two spots on the surface of a single fiber to evaluate the elemental compositions.

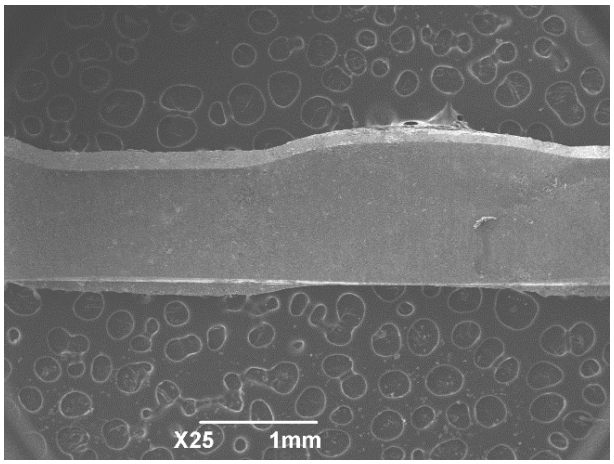

Figure 41. Free end of steel fiber

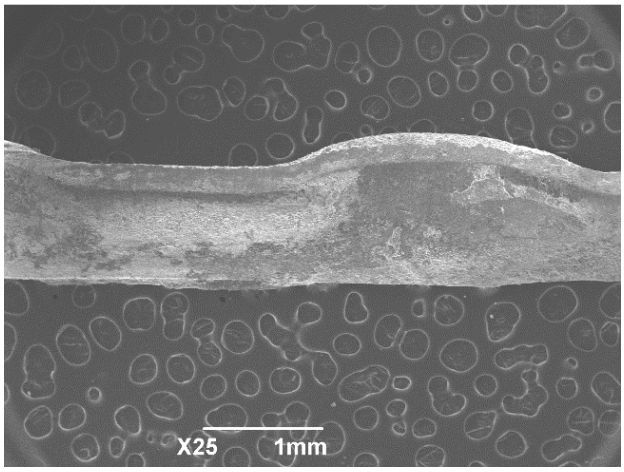

Figure 42. Pulled out end of steel fiber

Figure 41, and 42 show the difference in the free end and pulled out end of a steel fiber in the pullout test. The free end of steel fiber was smooth with a uniform cross-sectional surface in the microstructure, but the pulled-out end displayed many uneven surfaces, and fractures which could be explained by the abrasion of the fiber with the surface of cement matrix. This can be explained by the geometry of the fiber with sharp edges allowing a strong mechanical interaction and frictional interlocking during the pull-out phase. There were deposits of cementitious materials observed on the pulled-out end of the fiber. Following Figures 43, 44 display different magnification levels of the pulled-out end.

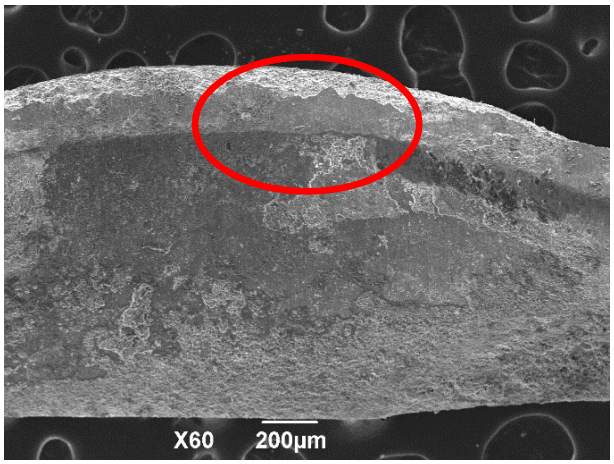

Figure 43. Pulled out end at X60 resolution

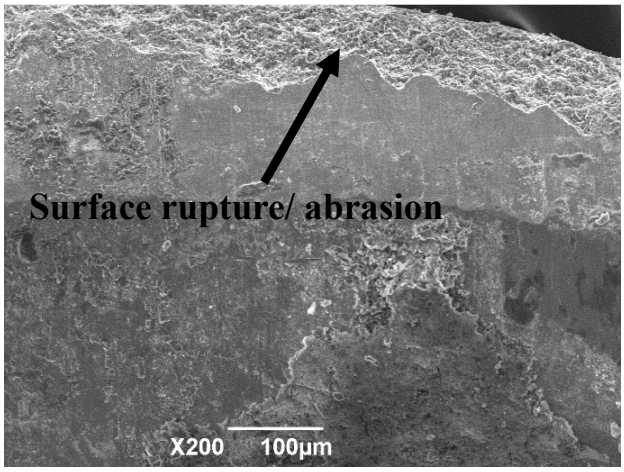

Figure 44. Surface abrasion on the fiber

Figure 44 is the 200x resolution enlargement of Figure 43, which was taken at 60x. The top edge of the fiber in Figure 43 shows a major fracture along the curve end indicating the rupture of the surface during pullout. The abraded steel fiber particles often provide a gradual increase in frictional resistance during the pullout phase thus explaining the slip hardening effect. The geometry of the fiber plays an important role in characterizing the friction between the fiber and matrix, as the mechanical interaction was observed mostly along the edges of the fiber. The surface area of the fiber showed deposits of matrix, indicating chemical bonding along the interphase.

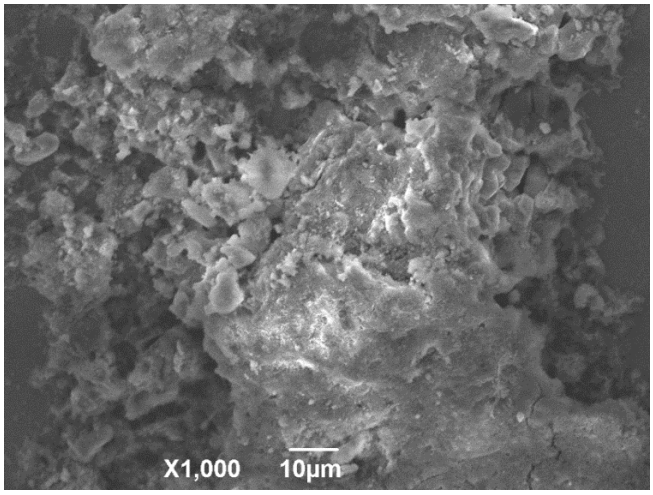

Figure 45. Cementitious material deposit on the fiber

Figure 45 shows deposited material on the fiber surface. The deposited material has a composite structure like that of a cementitious system, and a considerable two-thirds of a 10 microns image was filled by lumps of matrix material. The presence of cementitious deposits on the fiber was validated by performing EDS testing on the pulled-out fibers. Figures 46 to 49 represent the BES image for the pulled-out end of steel fiber followed by EDS analysis for the different areas marked on the fiber surface.

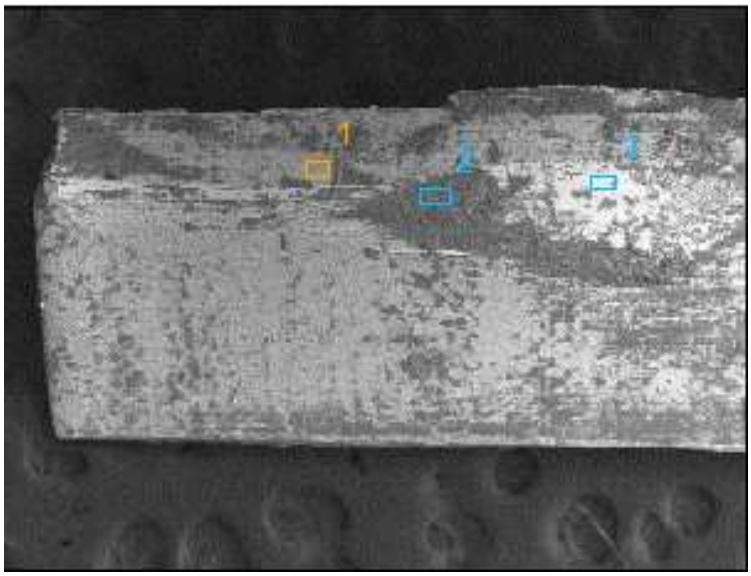

Figure 46. BES image for pulled out end of steel fiber

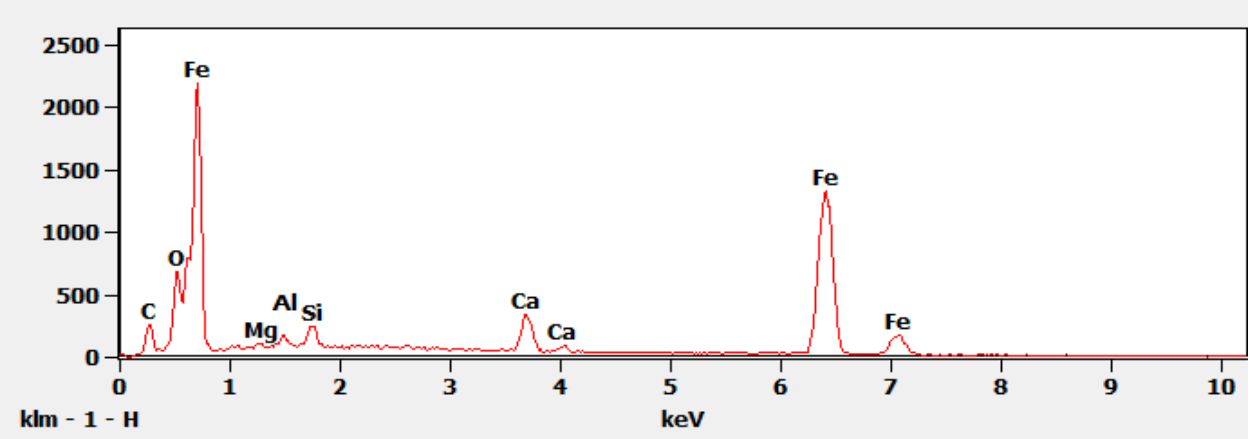

Figure 47. Elemental composition for spot 1 in figure 46

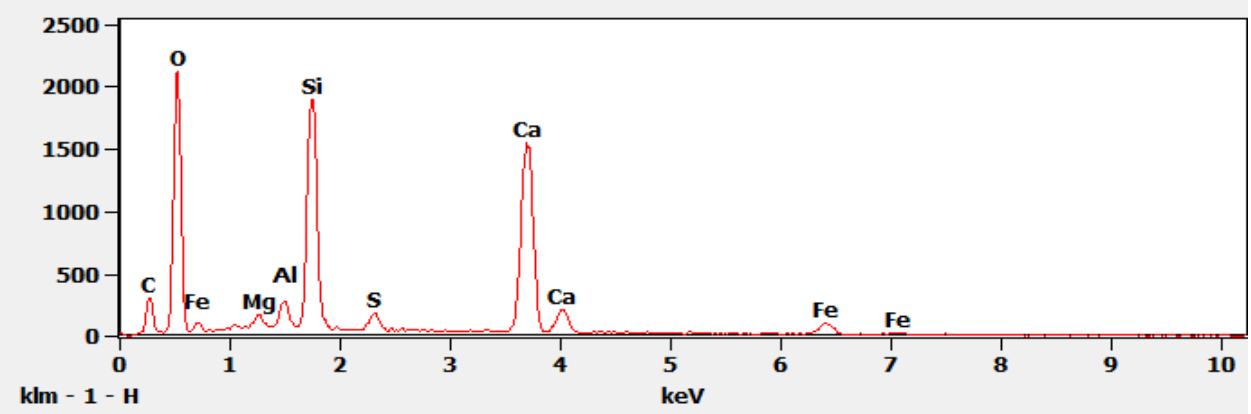

Figure 48. Elemental composition for spot 2 in figure 46

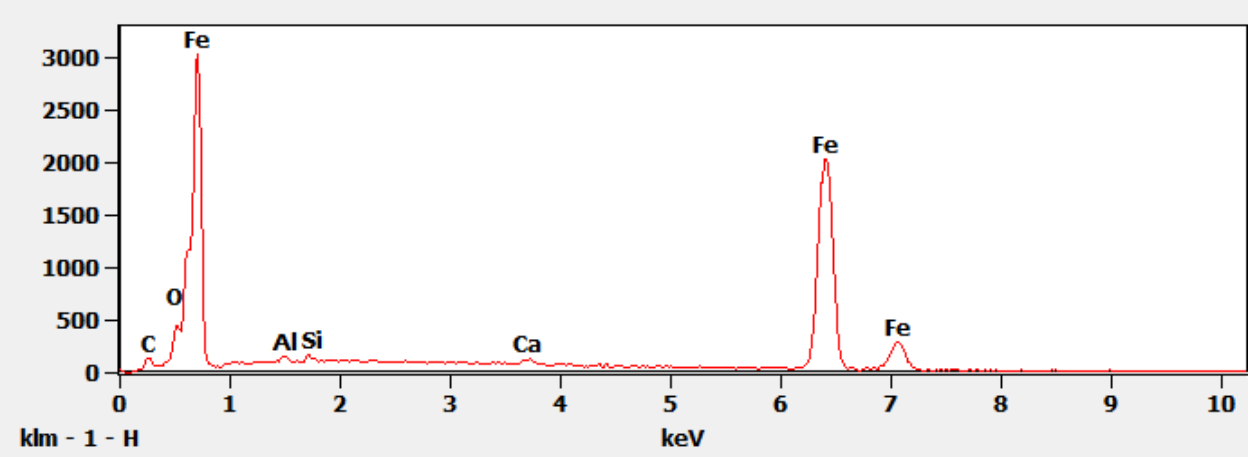

Figure 49. Elemental composition for spot 3 in figure 46

The image in Figure 46 shows the pulled-out end of a steel fiber analyzed for chemical deposits at three different places on its surface. A typical practice in EDS analysis is to observe the difference in brightness along the subject area to decode the chemical composition. The first and third shots were fairly brighter spots compared to the second shot. The major difference observed in the elemental composition results obtained for the first and third shots against the second shot was that of Fe. Figure 48 reports a low value of Fe compared to the other elements in the breakdown. Elements O, Si, and Ca, apparently the trivial components of a cementitious system's hydration product forming calcium silicates, calcium hydroxide and silica, indicate that the deposited material at Spot 2 was a cementitious composite. This chemical deposit on the steel surface fiber has shielded the major Fe component in steel composition from exposure to energy dispersion. There were no major changes seen in compositions of other elements such as Aluminum, Magnesium and Carbon since the weight percentages of these elements in the stainless-steel fiber design mix was significantly lower than that of Fe. The process was repeated for two other specimens of pulled out steel fibers with a minimum of three investigative spots for each. Highly similar results were obtained for the rest of the test specimens, with a common observation made for high concentrations of Ca, Si, and O in darker regions against a high concentration of Fe in brighter part of the fiber surface.

The following Figures show electron microscopy testing images of pulled out polypropylene fibers. These fibers show a dispersive fibrous nature compared to that of steel fibers earlier tested due to their manufacturing process. Steel fibers were manufactured through melting and extracting process into single filaments, while the obtained polypropylene fibers were embossed from virgin polypropylene filaments. So, the resulting polypropylene fiber is a multifilament structure stitched together from propriety blend of polypropylene resins.

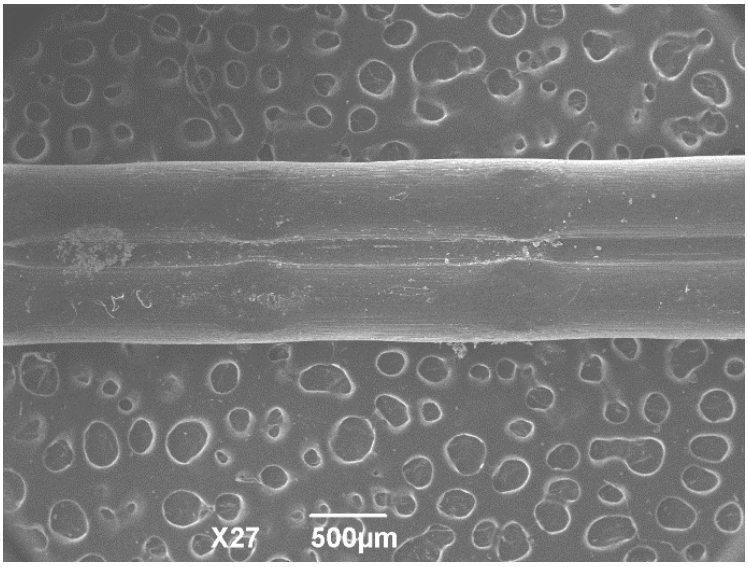

Figure 50. Free end of polypropylene fiber

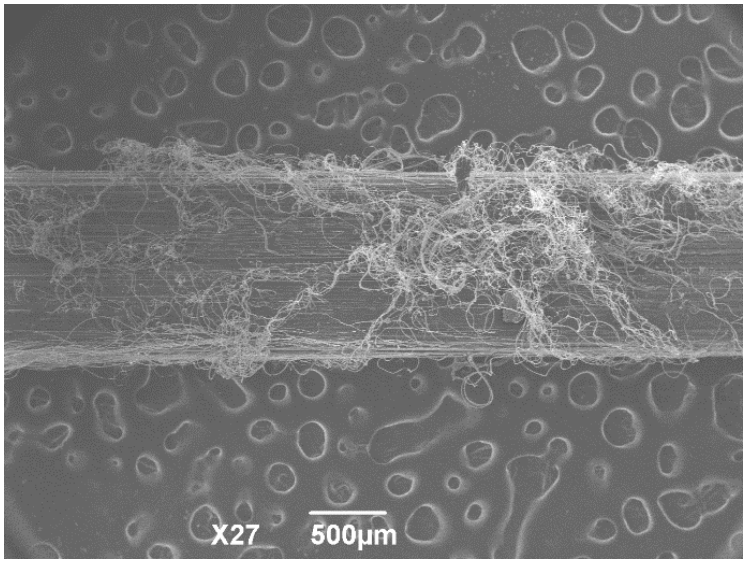

Figure 51. Pulled out end of polypropylene fiber

The figures show a clear understanding of the chemical and mechanical forces acting on the fiber towards the embedded end. The fiber has a complex structure with some blended filaments running through its length separated by a ridge in the center. This allows the fiber to rupture showing a tendency for splitting during the pullout phase of the fiber as seen in Figure 51. The pulled-out end reports a cluster of splits from the fiber's structure, implying a strong mechanical interaction between the fiber and matrix during the pullout. Figures 52, 53, and 54

provide a better understanding through higher resolutions, that were used to capture any unfamiliar and alien deposits on the fiber surface. There were lower concentrations of deposits on these fibers found in the images below in comparison to steel fibers, indicating that the steel fibers exhibit a better chemical bonding with cement matrix than polypropylene fibers. The splits on the fiber surface decreases the surface area of the fiber gradually during the pullout phase, which explains the reason for a decrease in the mechanical interaction of the fiber with matrix. These images for polypropylene fibers have also showed minute granular deposits of matrix materials tangled among the resin splits which might be a considerable factor for a frictional interaction. However, granular particles which were of the size of $1/100^{th}$ of a micrometer resolution image held in a static position by the polypropylene resin splits impedes the dynamic motion of the abraded particles leading to a constant deceleration in frictional force during the pullout. The results of the single fiber pullout tests, peel tests and the new method proposed comply with the previous statement.

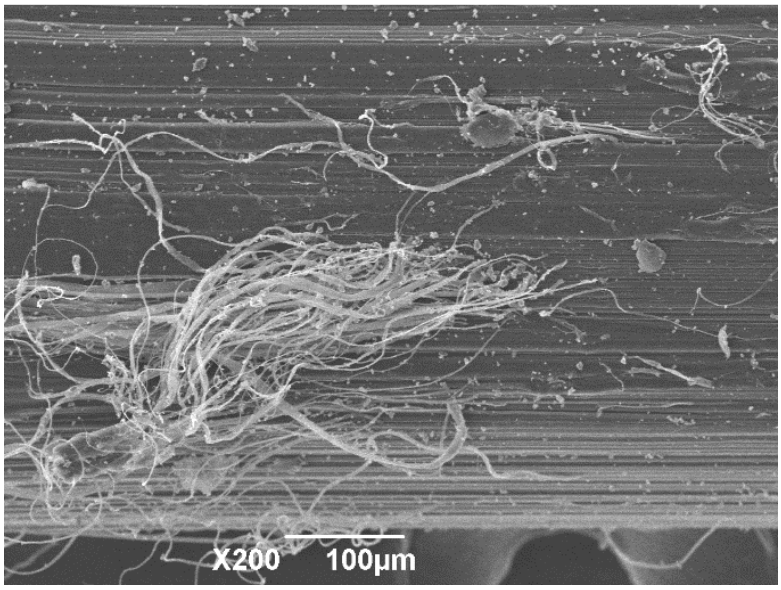

Figure 52. Fibrillation effect in polypropylene fiber

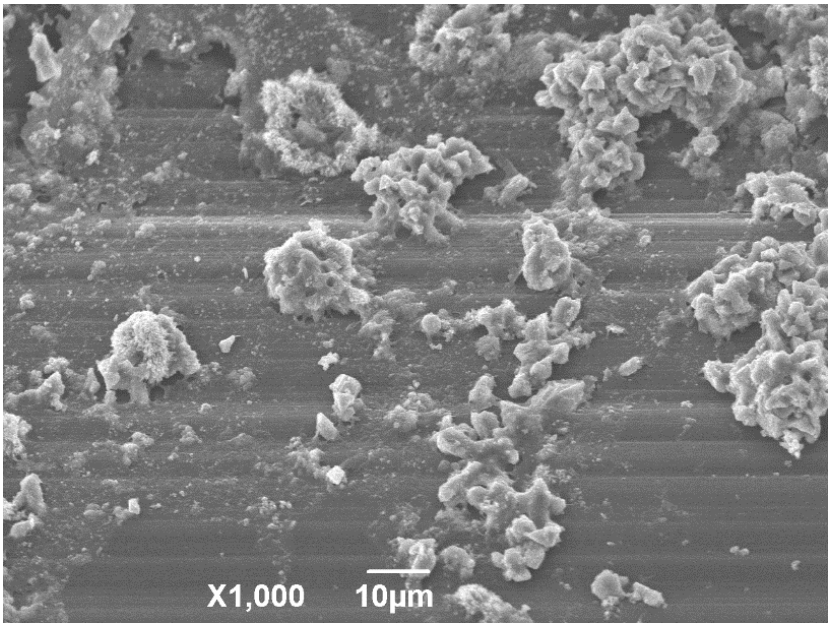

Figure 53. Cementitious deposits on polypropylene fiber surface

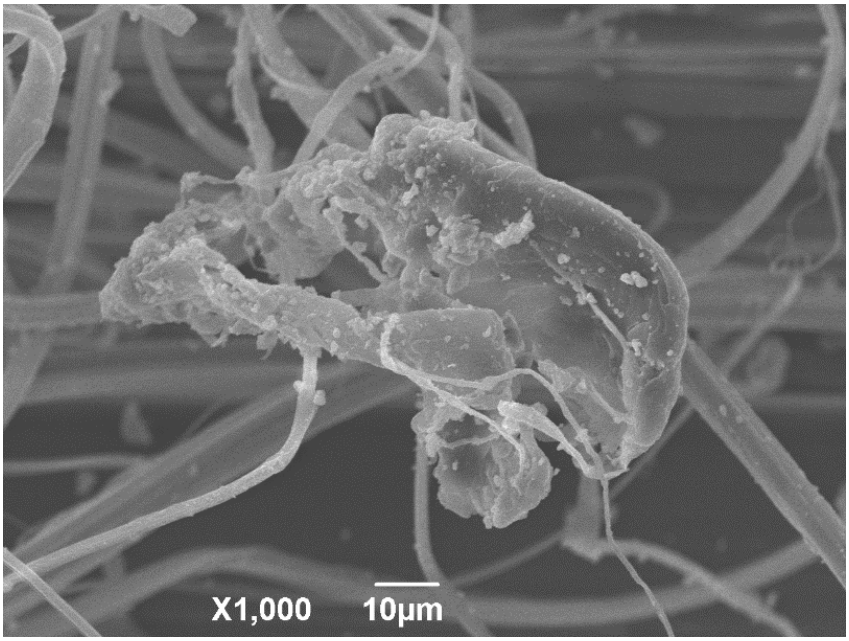

Figure 54. Granular deposits on the split polypropylene resin

EDS analyis for the polypropylene fibers was discussed from Figures 55 to 60 with BES image followed by images with a breakdown of elemental compositions of the five investigated areas shown. The polypropylene fibers used in this study were translucent, with poor conductivity and reflectivity for optical and energy rays. So, the polypropylene fibers were gold coated before

SEM and EDS analysis to improve their abiltiy to yield results in the testing procedures. This explains the appearance of Au composition in the analysis.

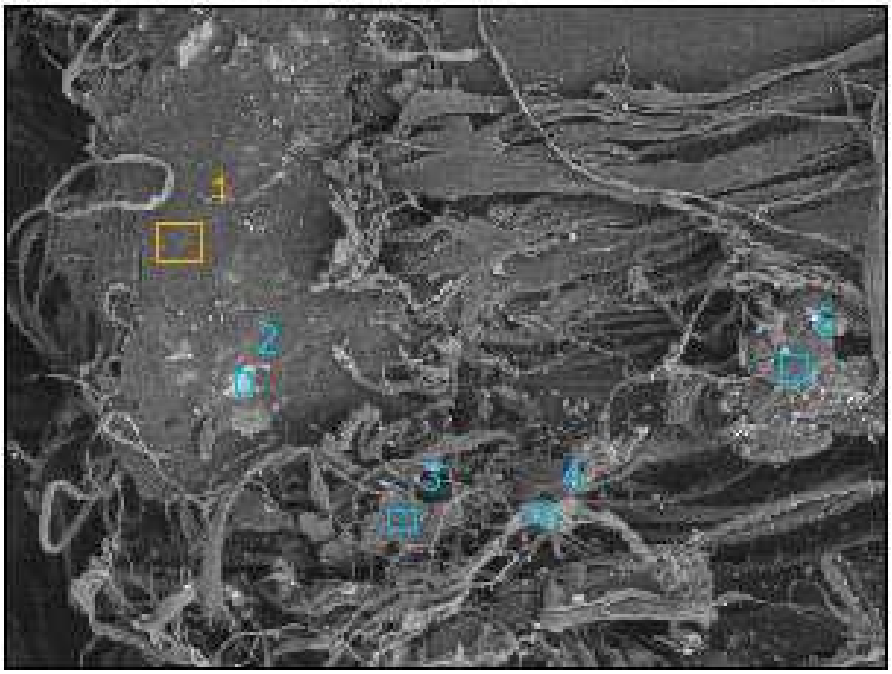

Figure 55. BES image for pulled out end of polypropylene fiber

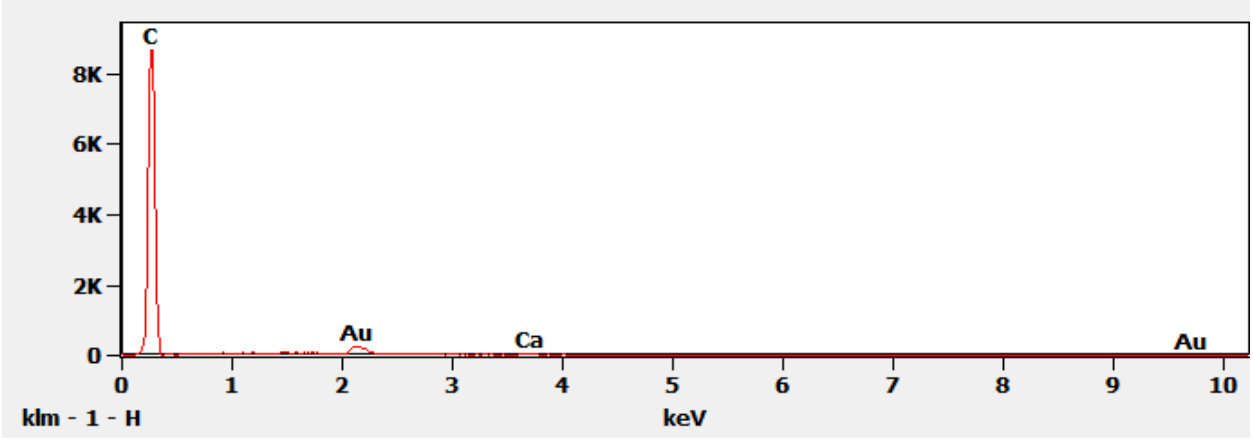

Figure 56. Elemental composition for spot 1 in figure 55

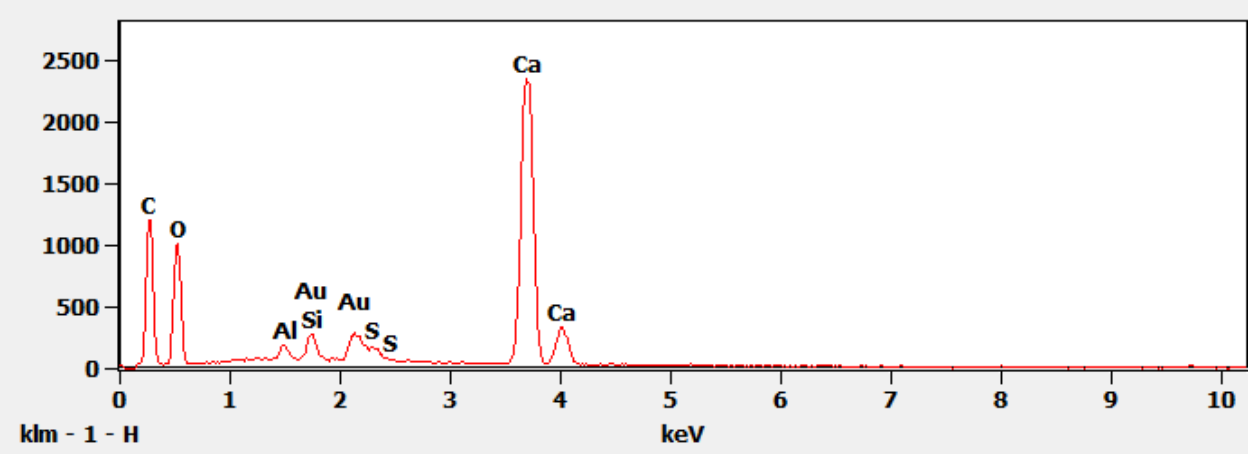

Figure 57. Elemental composition for spot 2 in figure 55

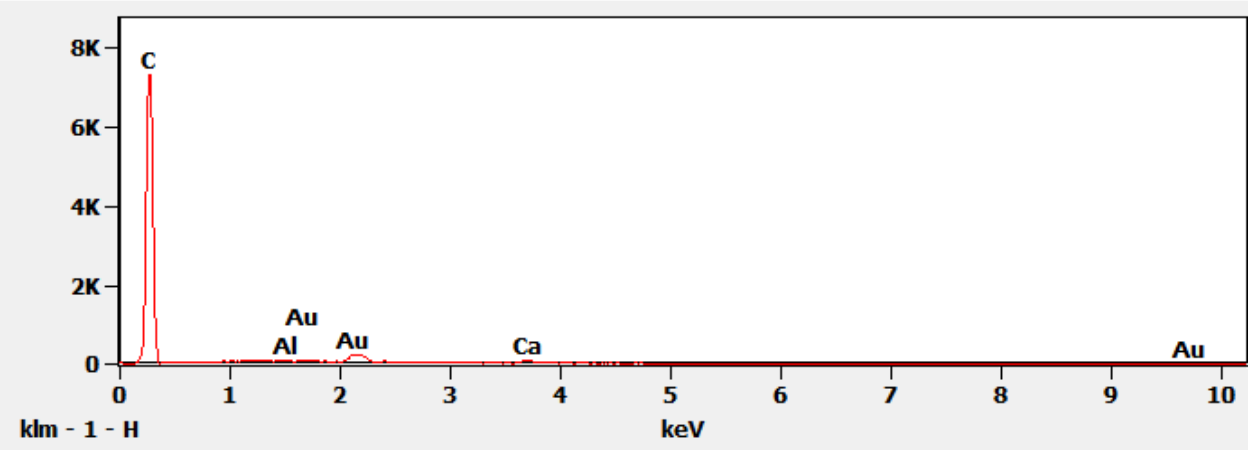

Figure 58. Elemental composition for spot 3 in figure 55

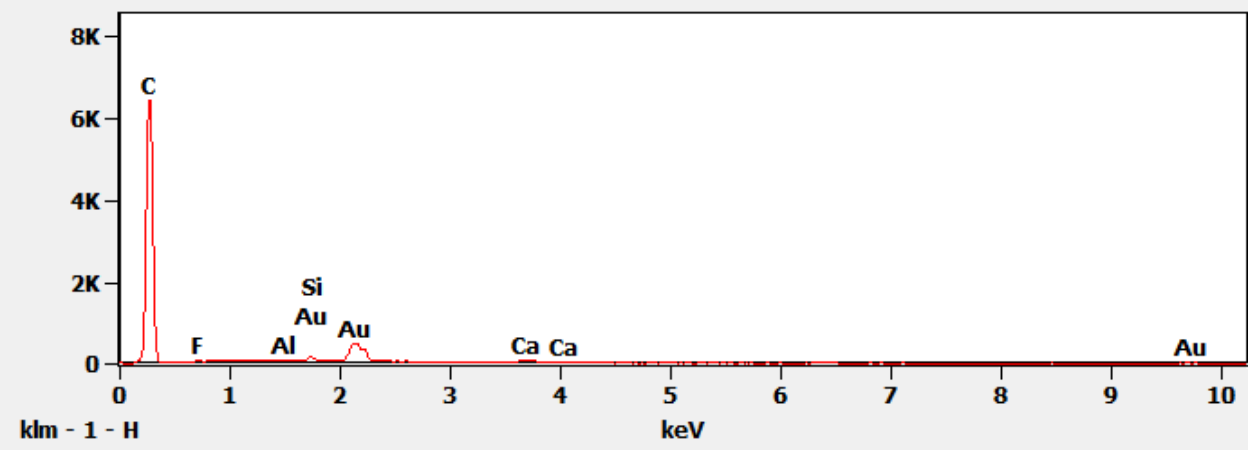

Figure 59. Elemental composition for spot 4 in figure 55

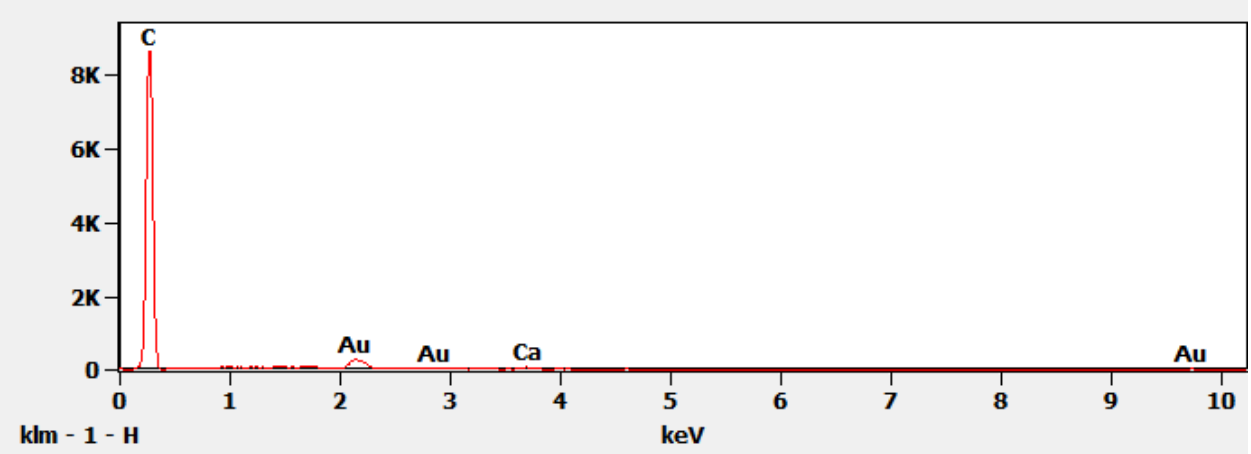

Figure 60. Elemental composition for spot 5 in figure 55

A 100µm magnified BES image shown in figure 55 contains few scattered bright spots constituting to a very low area compared to the darker surface of the fiber which forms the significant part of the total area of the image, indicating that the granular deposits of the cementitious particles have been dispersed in poor concentration compared to that seen in figure 45 for steel fiber. Among the five investigated areas, spot 2 was the only area that comprised of low carbon composition. The rest of the areas displayed very high composition of carbon. The fiber being polypropylene with a chemical formula of $(C_3H_6)_n$ narrows down to yield high compositions of carbon in EDS analysis. Spot 2 was the brightest among all five spots, hence the variation in elemental compositions from the rest. This was the only area that showed adequate amounts of Ca, Si, and O to form calcium silicates and other hydration compounds of cementitious systems. The probability of this chemical deposit is 0.2 in an image of 100µm magnification, which explains the poor chemical bonding of the fiber with a cementitious system. Two more test specimens were examined using the same analysis and yielded similar results. Polypropylene fibers have shown a weak chemical bonding with the matrix, which makes mechanical interaction the decisive factor for interfacial bond strength in polypropylene- cementitious composites.

Peel Test Results

Results for peel tests are discussed in this section. Peel tests were typically used for academic and industrial purposes to evaluate the adhesive bond strength of an adhesive with a medium. In this research study, fibers were peeled off cementitious matrix to determine their peel strength, which in turn was used to characterize the fiber-matrix's interfacial bond strength. Raw data was collected from Trapezium X software for peel load against the peel length and were plotted on a graph, as shown in Figures 11 and 12. There were five specimens tested for both fiber types, polypropylene and steel. The peel lengths recorded for each specimen were observed to be different and less than the common embedded length of 5mm.

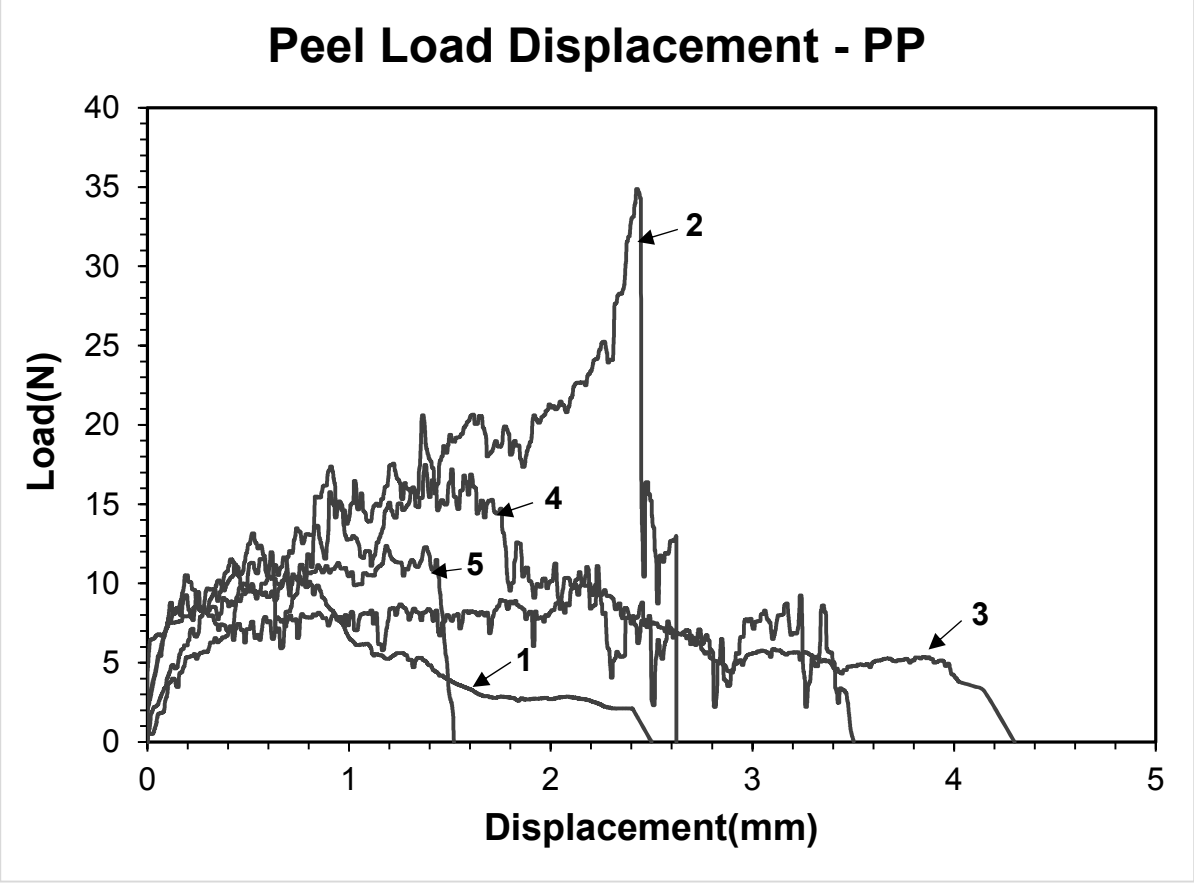

Figure 61. Peel test curves for polypropylene fibers

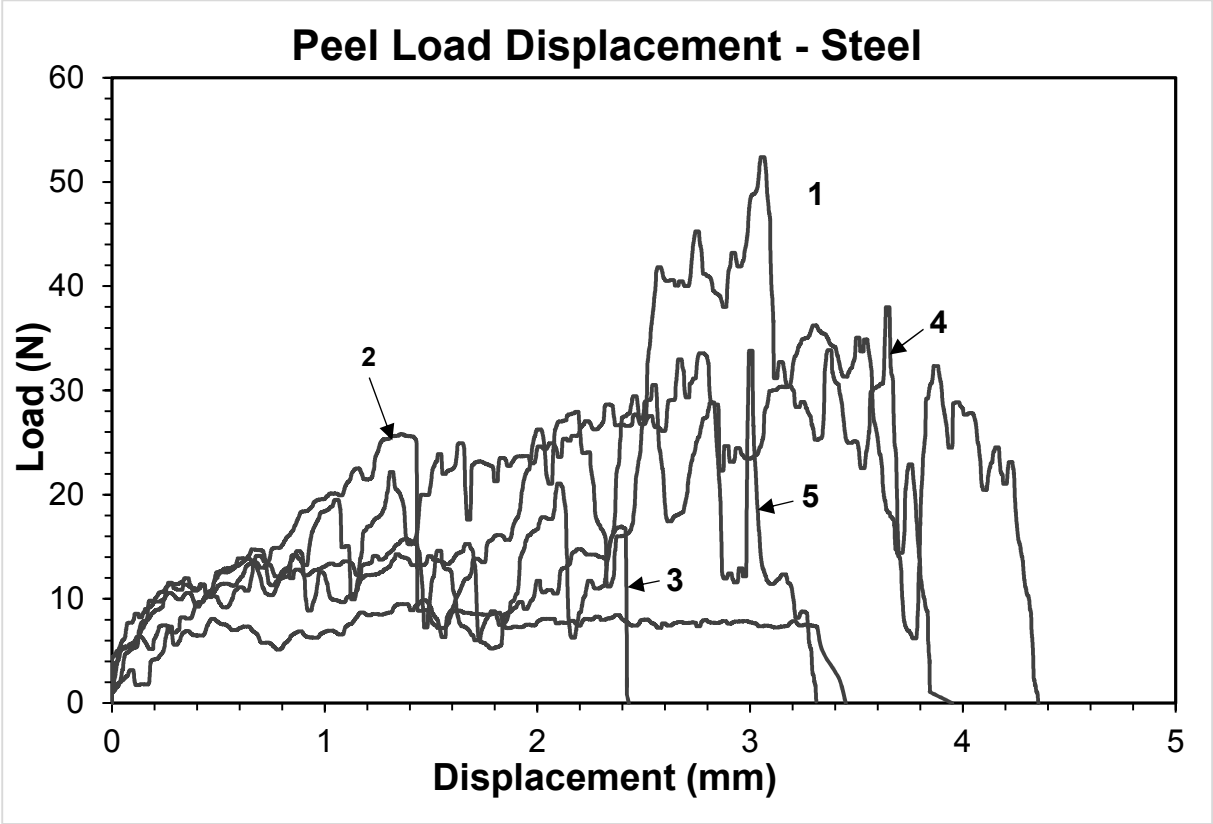

Figure 62. Peel test curves for steel fibers

Peel tests were an experimental study as conducted in this research. Repeatability for peel test curves was observed to be similar for steel and polypropylene test specimens, where three out of five curves were consistent for the peel displacement and peak peel load observed.

Peel Strengths for adhesives were usually calculated from the equation $Peel\ Strength = Average\ Peel\ Load / Conductor\ Width$, where average peel load for a specimen is the average of all the load values throughout its peel length, and conductor width is the contact width. This holds good for adhesives as they are 2-D materials with a linear dimension in contact with the medium when peeled off. But, for fibers the contact with medium is surface area, hence the previous equation was modified to evaluate the bond strength as $Peel\ Strength\ of\ fiber = Average\ Peel\ Load/(Contact\ area\ for\ peeling)$.

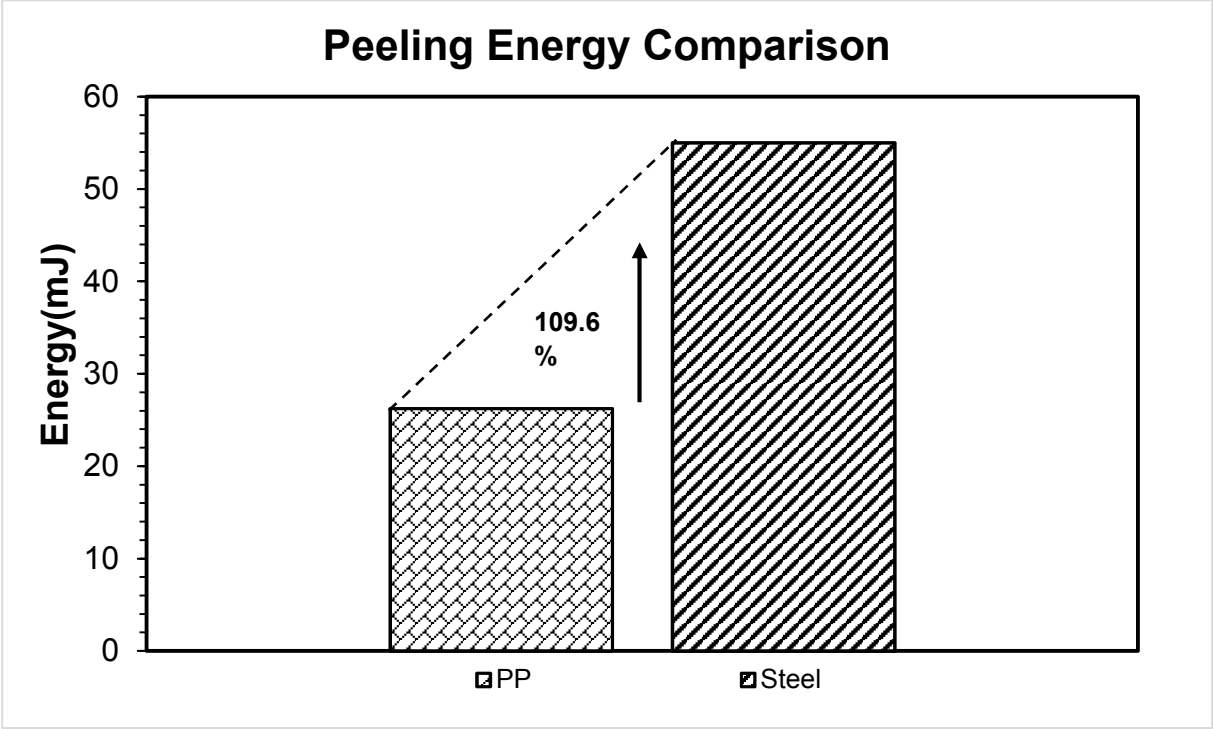

Figure 63. Average peeling energies comparison chart

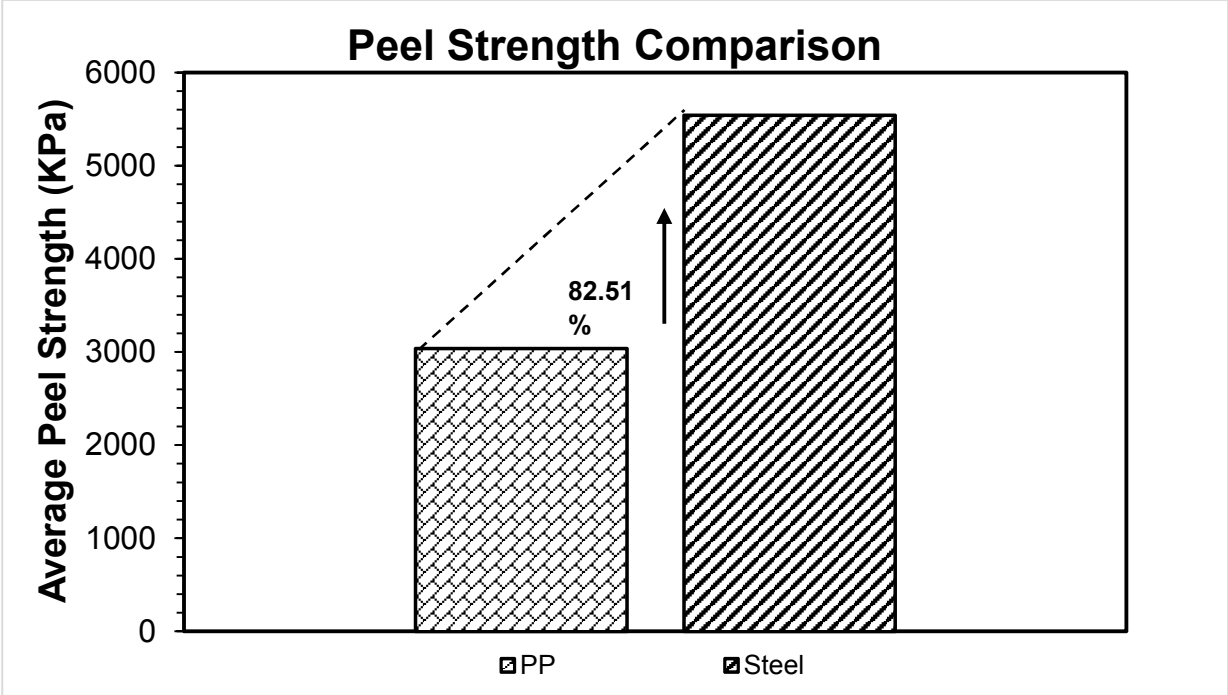

Figure 64. Average peel strength comparison chart

Figures 63, and 64 represent the average peeling work chart, and average peeling strength comparison chart for steel and polypropylene fibers. The average peeling energy and peel strength for steel fibers were higher than polypropylene fibers as noticed. The average peeling energy required to peel off steel fibers from cementitious system was 109.6% higher than that of polypropylene fibers, see Figure 13. On a similar note, it was observed that steel fibers showed peel strength of 5544KPa which is 82.5% higher than that of polypropylene fibers at 3037KPa.

CONCLUSIONS

1. A modified pullout method was proposed for investigating the interfacial bond parameters (pullout load, pullout energy, and frictional bond strength) between a natural fiber and a cementitious system. The new method was performed for pullout on steel and polypropylene fibers as well, for a comparison analysis among all the fibers chosen in the study. The modified pullout test focused on providing a minimal elastic bonding between the fiber and matrix, to observe frictional bonding as the dominant mechanism at the fiber-matrix interface in the pullout test. Results for interfacial bond strength have shown that wheat straw fiber frictional bond strength with the cementitious system to be independent of the embedment length in the pullout test.
2. Detailed understanding of the relationship between surface roughness of fibers and their corresponding interfacial frictional bond strengths was achieved, by maintaining the other influential parameters constant. Surface roughness studies have shown an order of roughness indices for fibers that are in compliance with the order of the frictional bond strength values observed in the modified pullout method, which validates the principle behind proposing the modified pullout method.
3. Standard single fiber pullout methods were conducted for steel and polypropylene fibers to evaluate their interfacial bond strength in a cementitious system with a water cement ratio of 0.485 cured for 7days. The typical behavior of fiber pullout curves from these test results were explained by Scanning Electron Microscopy (SEM) and Energy Dispersive Spectroscopy (EDS) analysis in conjunction, which showed similarities with the literature studies.
4. Peel tests were introduced for fiber cementitious system as a pilot study. The peel parameters for fibers were observed to be in compliance with the pullout parameters from other tests.

LIMITATIONS AND FUTURE WORK

1. Steel fibers selected in this research work were mechanically deformed, causing a need to study the additional mechanical anchorage provided by undulations on the fibers. A macro-mechanical study of fiber surface characteristics in conjunction with the current micro-surface profile studies would provide a comprehensive understanding of interfacial bond parameters in the modified pullout tests. The manufactured design for polypropylene fibers used individual monofilaments to bundle them into single entity, which changes fiber-matrix dynamics when studying about interfacial bond behavior. Hence, a macro-mechanical investigation needs to be done for polypropylene fibers due to their bundling nature.
2. The surface profilometry adopted in this research study to investigate the roughness characteristics of fibers was done using a stylus mechanism, which is capable of producing a unidimensional profile. However, there is a need to investigate the 2-D topography of fiber's surface characteristics for an optimal validation of the new pullout test proposed.
3. The minimization of the elastic bond needs to be quantified in the modified pullout method. Wheat straw fibers used in this research were untreated, and relevant accommodations must be made in the new pullout test to account for their water absorbing capacity. More pullout tests need to be done with different natural fibers and different treatments to understand the effect of surface roughness on interfacial bond strength.
4. Peel tests experimented on this study need to be standardized with specimen preparation, and testing techniques. The bond-slip mechanism in these tests also needs to be investigated, validated, and modeled for unconventional peeling specimens such as fibers in this case.

REFERENCES

Abbas, M., & Khan, M. (2016). Fiber-matrix interfacial behavior of hooked-end steel fiber-reinforced concrete. *Journal of Materials in Civil Engineering*, 10.

Abu-Lebdeh, T., Hamoush, S., Heard, W., & Zornig, B. (2011). Effect of matrix strength on pullout behavior of steel fiber reinforced very-high strength concrete composites. *Construction and Building Materials*, 39-46.

ACI commitee. (2005). *State of art report on synthetic fiber reinforced concrete.* Farmington Hills: American Concrete Institute.

Alwan, J., Naaman, A., & Hansen, W. (1991). Pull-out work of steel fibers from cementitious composites: Analytical investigation. *Cement & Concrete Composites*, 247-255.

Babafemi, A., & Boshoff, W. (2017). Pull-out response of macro synthetic fibre from concrete matrix: Effect of loading rate and embedment length. *Construction and Building Materials*, 590-599.

Banthia, N., & Trottier, J.-F. (1994). Concrete reinforced with deformed steel fibers, Part 1: Bond-slip mechanisms. *ACI Materials*, 435-446.

Bentur, A., & Mindess, S. (2006). *Fiber reinforced cementitious composites.* CRC Press.

Chamis, C. C. (1972). *Mechanics of load transfer at fiber/matrix interface.* National Aeronautics and Space Administration.

Choi, J.-I., & Lee, B. Y. (2015). Bonding properties of basalt fiber and strength reduction according to fiber orientation. *MDPI materials*, 6719-6727.

Choi, W.-C., Jang, S.-J., & Yun, H.-D. (2015). Interface bond characterization between fiber and cementitious matrix. *International Journal of Polymer Science*, 11.

Fantilli, P., & Paolo, V. (2007). A cohesive interface model for the pullout of inclined steel fibers in cementitious matrixes. *Journal of advanced concrete technology*, 247-258.

Gokoz, U. N., & Naaman, A. E. (1981). Effect of strain-rate on the pull-out behaviour of fibres in mortar. *International Journal of Cement Composites and Lightweight Concrete*, 187-202.

Isla, F., Ruano, G., & Luccioni, B. (2015). Analysis of steel fibers pull-out. Experimental study. *Construction and Building Materials*, 183-193.

Jewell, R. B., Mahboub, K. C., Robl, T. L., & Bathke, A. C. (2015). Interfacial bond between reinforcing fibers and calcium sulfoaluminate cements: Fiber pullout characteristics. *Civil Engineering Faculty Publications*, paper 5.

Kanda, T., & Li, V. C. (1998). Interface property and apparent strength of high-strength hydrophilic fiber in cement matrix. *Journal of materials in civil engineering*, 5-13.

Katz, A., & Li, V. (1996). A special technique for determining the bond strength of micro-fibers in cement matrix by pullout method. *Journal of materials science letters*, 1821-1823.

Katz, A., Bentur, A., Alexander, M., & Arliguie, G. (1998). *The interfacial transitional zone in cementitious composites.* Haifa: E & FN Spon.

Kim, D. J., El-Tawil, S., & Naaman, A. E. (2008). Loading rate effect on pullout behavior of deformed steel fibers. *ACI materials*, 576-584.

Leung, C., & Li, V. (1990). Applications of two way debonding theory to short fiber composites. *Composites*, 305-317.

Li, V. C., & Lin, Z. (1996). Crack bridging in fiber reinforced cementitious composites with slip-hardening interfaces. *Journal of mechanics and physics of solids*, 763-787.

Li, V. C., & Stang, H. (1997). Interface property characterization and strengthening mechanisms in fiber reinforced cement based composites. *Advanced Cement Based Materials*, 1-20.

Li, V. C., Wang, Y., & Backer, S. (1991). A micromechanical model of tension-softening and bridging toughening of short random fiber reinforced brittle matrix composites. *Journal of mechanics and physics of solids*, 607-625.

Li, V., Wang, Y., & Backer, S. (1990). Effect of inclining angle, bundling and surface treatment on synthetic fiber pull-out from a cement matrix. *Composites*, 132-140.

Marshall, D., & Cox, B. (1985). The mechanics of matrix cracking in brittle-matrix fiber composites. *Acta Metallurgica*, 2013-2021.

Marshall, D., & Cox, B. (Acta Metallurgica). Tensile fracture of brittle matrix composites: influence of fiber strength. *1987*, 2607-2619.

Naaman, A. E., & Shah, S. P. (1976). Pullout mechanism in steel fiber reinforced concrete. *Journal of the Structural Division*, 1537-1548.

Naaman, A., & Willie, K. (2012). Bond stress-slip behavior of steel fibers embedded in ultra high performance concrete. *ACI Materials*, 479-488.

Nepal, B. &. (2015). A review on agricultural fiber reinforced concrete. *Sustainable Buildings and Structures*, (pp. 125-130).

Obla, K. H., & Li, V. C. (1995). A novel technique for fiber-matrix bond strength determination for rupturing fibers. *Cement & Concrete Composites*, 219-227.

Onuaguluchi, O., & Banthia, N. (2016). Plant-based natural fiber reinforced cement composites: A review. *Cement and Concrete Composites*, 96-108.

Pacios, A., Ouyang, C., & Shah, S. (1995). Rate effect on interfacial response between fibers and matrix. *Materials and structures*, 83-91.

Shannag, J. M., Brincker, R., & Hansen, W. (1997). Pullout behavior of steel fibers from cement-based composites. *Cement and Concrete Research*, 925-936.

Singh, S., Shukla, A., & Brown, R. (2004). Pullout behavior of polypropylene fibers from cementitious matrix. *Cement and Concrete Research*, 1919-1925.

Swamy, R. (1980). Prospects of fiber reinforcement in structural applications, in advaces in cement-matrix composites. *Materials Research Society*, 159-169.

Vorburger, T., & Raja, J. (1990). *Surface Finish Metrology Tutorial.* Gaithersburg: National Institute of Standards and Technology.

Wang, Y., Backer, S., & Li, V. C. (1987). An experimental study of synthetic fiber reinforced cementitous composites. *Journal of Materials Science*, 4281-4291.

Wang, Y., Li, V. C., & Backer, S. (1988). Modeling of fiber pull-out from cement matrix. *The international journal of cement composites and lightweight concrete*, 143-149.

Wang, Y., Li, V., & Backer, S. (1987). Analysis of synthetic fiber pull-out from cement matrix. *MRS Proceedings*, 114-159.

Wei, S., Mandel, J. A., & Said, S. (1986). Study of the interface strength in steel fiber reinforced cement based composites. *Journal of the american concrete institute*, 597-605.

Zile, E., & Zile, O. (2013). Effect of the fiber geometry on the pullout response of mechanically deformed steel fibers. *Cement and Concrete Research*, 18-24.

APPENDIX

Modified Pullout Tests

Table A1

Pullout load and pullout energies for polypropylene fibers in modified pullout method

Specimen	10mm embedment		20mm embedment	
	Pullout load (mN)	Pullout energy (mJ)	Pullout load (mN)	Pullout energy (mJ)
1	51.4	0.437	57.53	0.697
2	46.06	0.337	57.79	0.741
3	54.32	0.385	64.5	0.802
4	57.08	0.511	53.71	0.647
5	45.7	0.378	65.11	0.85
6	48.67	0.433	50.48	0.652
7	50.59	0.321	28.16	0.391
8	47.08	0.437	33.39	0.421
Average Values	50.1125	0.404875	51.33375	0.650125

Table A2

Pullout load and pullout energies for steel fibers in modified pullout method

Specimen	10mm embedment		20mm embedment	
	Pullout load (mN)	Pullout energy	Pullout load (mN)	Pullout energy (mJ)
1	59.5	0.286	87	0.805
2	51.5	0.271	65	0.46
3	51	0.234	58	0.581
4	93.875	0.309	80	0.501
5	50.687	0.289	110	0.533
6	47	0.288	60	0.526
7	54	0.275	82	0.804
8	40.98	0.24	95	0.725
Average Values	56.06775	0.274	79.625	0.616875

Table A3

Pullout load and pullout energies for wheat straw fibers in modified pullout method

Specimen	10mm embedment		20mm embedment	
	Pullout load (mN)	Pullout energy (mJ)	Pullout load (mN)	Pullout energy (mJ)
1	0.1846	0.855	0.334	2.82
2	0.13438	0.266	0.423	2.458
3	0.1509	0.623	0.193	0.944
4	0.146015	0.697	0.345	2.558
5	0.19965	0.846	0.344	2.761
6	0.14002	0.462	0.23	2.72
7	0.21434	0.43	0.371	2.202
8	0.15763	0.707	0.325	3.27
Average Values	165.941875	0.61075	320.625	2.466625

Table A4

Interfacial bond strength comparison in modified pullout method (KPa)

Specimen	Polypropylene		Steel		Wheat straw	
	10mm	20mm	10mm	20mm	10mm	20mm
1	0.00197	0.00114	0.0038	0.00294	0.00299	0.00282
2	0.00188	0.00115	0.00329	0.0022	0.00221	0.00343
3	0.00214	0.00128	0.00326	0.00196	0.00242	0.00161
4	0.00222	0.00107	0.00605	0.00267	0.0023	0.00286
5	0.00179	0.00132	0.00324	0.00358	0.00318	0.00279
6	0.00186	0.00101	0.00301	0.00194	0.00217	0.00187
7	0.00201	0.00056	0.00347	0.00262	0.00329	0.00302
8	0.00177	0.00066	0.00263	0.00279	0.00251	0.00267
Average Values	1.95367	1.02253	3.5937	2.5872	2.63489	2.63414

Standard Single Fiber Pullout Tests

Table A5

Peak loads and total energies for steel fibers in standard single fiber pullout test

Specimen	Pullout energy (mJ)	P_b - Frictional Load (N)	Debonding energy (mJ)	P_a - Peak debond load (N)
1	210.7285	105.5009	155.2715	137.7497
2	131.7783	93.72807	64.2217	99.72668
3	78.078	30.2406	26.922	42.13
4	55.8657	41.2051	11.1343	55.61383
5	281.7912	107.5261	163.2088	164.608
6	37.6862	19.2604	6.3138	36.00915
7	65.6804	31	76.3196	50.64
Average Values	123.0869	61.20873857	71.9131	83.78248

Table A6

Peak loads and total energies for polypropylene fibers in standard single fiber pullout test

Specimen	Pullout energy (mJ)	P_b - Frictional load (N)	Debonding energy (mJ)	P_a - Peak debond load (N)
1	123.2077	38.624	153.7923	88.23
2	51.446	1.76668	66.554	61.59
3	8.4713	4.27405	50.5287	51.21
4	104.499	17.9879	107.501	74.85
5	2.868	12.5672	65.132	53.08
6	13.827	5.73349	57.173	45.99
7	42.8	1.9089	53.2	45.51
Average Values	49.58842857	11.83746	79.12585714	60.06571429

Table A7

Frictional bond strength values for polypropylene fibers in standard single fiber pullout test

Specimen	P_b - Frictional load (N)	End slip (mm)	Bond area (mm^2)	Bond strength (KPa)
1	38.624	8.874125	24.18955	159.6722552
2	1.76668	8.0504	24.18955	73.034844
3	4.27405	3.174375	24.18955	176.689934
4	17.9879	8.422501	24.18955	743.622763
5	12.5672	3.693375	24.18955	519.530128
6	5.73349	4.249125	24.18955	237.023425
7	1.9089	7.9545	24.18955	78.914242
Average Values	11.83746	6.345485857	24.18955	489.3625553

Table A8

Frictional bond strength values for steel fibers in standard single fiber pullout test

Specimen	P_b - Frictional load (N)	End slip (mm)	Bond area (mm^2)	Bond strength (KPa)
1	105.5009	5.8958	15.7	6719.802548
2	93.72807	3.75725	15.7	5969.940764
3	30.2406	4.057875	15.7	1926.152866
4	41.2051	3.239775	15.7	2624.528662
5	107.5261	5.175	15.7	6848.796178
6	19.2604	2.68725	15.7	1226.77707
7	31	3.87975	15.7	1974.522293
Average Values	61.20873857	4.098957143	15.7	3898.645769

Peel Tests

Table A9

Peel parameters for polypropylene fibers in peel tests

Specimen	Peel load (N)	Peeling work(mJ)	Peel strength(MPa)
1	5.64704459	13.686	1.868490226
2	15.6850806	41.15245	4.945793763
3	6.96136901	28.70642	1.339170342
4	9.86105973	34.538	2.329005786
5	8.64698245	13.128	4.705769085
Average Values	9.36030728	26.242174	3.03764584

Table A10

Peel parameters for steel fibers in peel tests

Specimen	Peel load (N)	Peeling work (mJ)	Peel strength (MPa)
1	19.517	85.004	5.709264684
2	10.9903	36.932	4.058081787
3	11.177	27.0702	5.859348379
4	20.4318	78.6361	6.589309038
5	14.307	47.3758	5.50452362
Average Values	15.28462	55.00362	5.544105502